UNIVERSITÉ DE LORRAINE

NORTHEASTERN UNIVERSITYSITY

DISSERTATION

Presented at
Université de Lorraine and Northeastern University
ZHANG Xiaoxue 张晓雪

To obtain the doctor's degree of
Université de Lorraine and Northeastern University

SPECIAL FIELD: Engineering Sciences
OPTION: Materials Science

Effects of high magnetic field on high purity Fe-C alloys during diffusional phase transformation

Defended on July 9th, 2012 in front of the jury:

Yevs Fautrelle	Professor	Institut National Polytechnique de Grenoble, France	Reviewer & Jury member
Zhongming Ren	Professor	Shanghai University, China	Reviewer & Jury member
Claude Esling	Professor	University of Lorraine, France	Supervisor
Tingju Li	Professor	Dalian University of Technology, China	Jury member
Philippe Martineau	Doctor	Service pour la Science et la Technologie, Ambassade de France en Chine， France	Jury member
Yuansheng Yang	Professor	Institute of Metal Research Chinese Academy of Sciences, China	Jury member
Liang Zuo	Professor	Northeastern University, China	Supervisor
Xiang Zhao	Professor	Northeastern University, China	Co-Supervisor
Yudong Zhang	Doctor HDR	University of Lorraine, France	Co-Supervisor

Laboratoire d'Étude des Microstructures et de Mécanique des Matériaux, LEM3
Ile du Saulcy 57045 Metz Cedex 1

Contents

Abstract

In this work, the influence of the magnetic field on diffusional phase transformation in high purity Fe-C alloys has been investigated theoretically and experimentally. The magnetic field induced microstructural features and crystallographic orientation characteristics have been thoroughly studied in three different carbon content alloys: Fe-0.12C, Fe-0.36C and Fe-1.1C alloys.

Magnetic field induces different aligned and elongated microstructures along the field direction, namely aligned and elongated pearlite colonies in Fe-0.12C alloy and elongated proeutectoid ferrite grains in Fe-0.36C alloy, due to the two scaled magnetic dipolar interaction. Magnetic field increases the amount of ferrite in hypoeutectoid alloys and this field effect becomes more pronounced with the increase of the carbon composition. Magnetic field inhibits the formation of Widmanstätten ferrite by introducing additional driving force to ferritic transformation and thus reducing the need for low energy interface which is required to overcome the transformation barriers during slow cooling process.

Magnetic field promotes the formation of abnormal structure by increasing the driving force of transformation from carbon-depleted austenite to ferrite and it enhances the spheroidization of pearlite due to its influence on accelerating carbon diffusion resulting from increased transformation temperature, together with its effect on increasing the relative ferrite/cementite interface energy.

The field induced enhancement of carbon solution in ferrite is evidenced through the WDS-EPMA measurements for the first time. *Ab-initio* calculations reveal that the presence of an interstitial carbon atom in bcc Fe modifies the magnetic moments of its neighboring Fe atoms. This leads to the decrease of the demagnetization energy of the system and makes the system energetically more stable under the magnetic field.

Due to the atomic-scaled magnetic dipolar interaction, magnetic field favors the nucleation and growth of the ferrite grains with their distorted <001> direction parallel to the transverse field direction, and thus induces the enhancement of the <001> fiber component in the transverse field direction. This field effect is related to the crystal lattice distortion induced by carbon solution and its impact becomes stronger with the increase of the carbon content and the field intensity.

Three ORs between pearlitic ferrite and cementite have been found in present work, namely Isaichev (IS) OR and two close Pitsch-Petch (P-P) ORs. Magnetic field hardly changes the types of the appearing ORs, but it considerably increases the occurrence frequency of the P-P2 OR, especially in Fe-1.1C alloy, by favoring the nucleation of ferrite.

Keywords: Magnetic Field, Phase Transformation, Magnetic Dipolar Interaction, Texture，Orientation Relationship

Résumé

Dans ce travail, l'influence du champ magnétique sur la transformation de phase diffusionnelle dans des alliages Fe-C de haute pureté a été étudiée théoriquement et expérimentalement. Les caractéristiques microstructurales et celles d'orientations cristallographiques induites par le champ magnétique ont été soigneusement étudiées dans trois alliages Fe-C à différents taux de carbone, à savoir Fe-0.12C, Fe-0.36C, Fe-1.1C.

Le champ magnétique induit différentes microstructures alignées et allongées le long de la direction du champ, à savoir des colonies de perlite alignées et allongées dans l'alliage Fe-0.12C et des grains allongés de ferrite proeutectoïde dans l'alliage Fe-0.36C, en raison de l'interaction magnétique dipolaire à deux différentes échelles. Le champ magnétique augmente la quantité de ferrite dans les alliages hypoeutectoïdes et cet effet du champ est plus prononcé avec l'augmentation du taux de carbone. Le champ magnétique inhibe la formation de ferrite de Widmanstätten en introduisant une force motrice supplémentaire pour la transformation ferritique et réduisant ainsi la nécessité de l'interface de faible énergie qui est requise pour surmonter les barrières de transformation durant le processus de refroidissement lent.

Le champ magnétique favorise la formation de la structure anormale en augmentant la force d'entraînement de la transformation de l' austénite appauvrie en carbone en ferrite et il améliore la sphereoidization de perlite en raison de son influence sur l'accélération de la diffusion de carbone entraînée par l'augmentation de la température de transformation, ainsi que son effet sur l'augmentation de l'énergie relative de l'interface ferrite /cémentite.

L'augmentation de la solubilité du carbone dans la ferrite induite par le champ est mise en évidence à travers les mesures WDS-EPMA pour la première fois. Des calculas ab-initio montrent que la présence d'un atome de carbone interstitiel dans Fe C modifie les moments magnétiques des atomes de Fe voisins. Ceci conduit à la diminution de l'énergie de démagnétisation du système et rend le système énergétiquement plus stable dans le champ magnétique.

En raison de l'interaction dipolaire magnétique à l'échelle atomique, le champ magnétique favorise la nucléation et la croissance des grains de ferrite ayant leur direction <001> distordue parallèle à la direction du champ transversal, et induit donc l'augmentation de la composante de fibre <001> dans le sens transversal par rapport à la direction du champ. Cet effet du champ est relié à la distorsion du réseau cristallin induite par une solution de carbone et son impact devient plus fort avec l'augmentation de la teneur en carbone et l'intensité du champ.

Trois relations d'orientations (OR) entre la ferrite perlitique et la cémentite ont été trouvées dans ce travail, à savoir l'OR Isaichev (IS) et deux OR proches des OR Pitsch-Petch (PP). Le champ magnétique ne modifie guère les types d'OR qui apparaissent, mais il augmente considérablement la fréquence d'occurrence des OR P-P2, en particulier dans l'alliage Fe-1.1C, en favorisant la nucléation de la ferrite.

Mots-clés: Champ magnétique, Transformation de phase, Interaction Dipolaire Magnétique, Texture, Relation d'Orientation

摘 要

本论文对强磁场下三种高纯铁碳合金（Fe-0.12C 合金, Fe-0.36C 合金 和 Fe-1.1C 合金）扩散型固态相变过程中显微组织形貌以及晶体学特征进行了系统的实验研究和理论解析。

研究发现，由于微观尺度和原子尺度上的磁偶极子相互作用, 强磁场能诱发亚共析钢中沿磁场方向排列和伸长的显微组织形貌的形成, 并且根据合金含碳量的不同, 显微组织形貌呈现不同特点。含碳量很低的 Fe-0.12C 合金中, 珠光体团呈沿磁场方向排列和伸长的趋势, 而 Fe-0.36C 合金中, 先共析铁素体呈沿磁场方向排列和伸长的形貌。由于强磁场对相平衡的影响, 使共析点含碳量升高, 导致强磁场下相变产物中铁素体含量明显增加，并且强磁场对铁素体转变的促进作用随合金含碳量的增加而增强。此外还发现，强磁场能明显抑制先共析魏氏体的形成。这是由于强磁场能提高铁素体相变驱动力，从而降低了依靠形成先共析魏氏体借助低能界面来克服相变阻力的需要。另外，强磁场通过提高铁素体相变驱动力，促进晶界渗碳体周围贫碳奥氏体的分解, 促进 Fe-1.1C 合金中反常组织的形成。同时，由于强磁场能提高珠光体相变温度, 促进碳原子扩散明显加快球化过程, 并通过提高铁素体/渗碳体界面能, 增加球化驱动力, 导致强磁场下 Fe-1.1C 合金中珠光体的球化趋势显著增加。

本研究从利用 WDS/EMPA 技术从实验上证实了强磁场能提高碳原子在铁素体中的溶解度。并利用第一性原理计算，模拟计算出碳原子对其周围铁原子磁矩的影响，从磁偶极子相互作用角度探寻磁场作用的物理本质。结果表明，溶解在铁素体中的间隙碳原子能显著降低其周围铁原子的原子磁矩, 降低系统中由于原子磁矩相互排斥而引起的退磁场能, 从而有利于提高系统的稳定性。

强磁场能诱发亚共析钢中先共析铁素体沿横磁场方向<001>织构的增强。在强磁场下，由于铁原子之间的磁偶极子作用, 使得平行于横磁场方向上的铁原子之间原子间距增大, 从而降低了由碳原子引起的晶格畸变能。因此, 强磁场对<001>方向平行于横磁场方向的铁素体晶粒的形核和长大过程有明显的促进作用, 导致横磁场方向上<001>织构的增强。由于该<001>织构的形成取决于由间隙碳原子引起的晶格畸变, 因此，该<001>织构的强度与合金含碳量以及磁场强度呈正比。

本论文中对珠光体的晶体学取向关系进行了研究，在每种合金中均发现了三种铁素体和渗碳体取向关系, 分别为 IS, P-P1 和 P-P2 取向关系。强磁场能促进高磁化率相-铁素体相的形核, 从而增加铁素体相优先形核的几率, 提高与铁素体相优先形核相对应的 P-P2 取向关系的出现几率。磁场的这一作用在 Fe-1.1C 合金中最为明显。但是, 强磁场对合金中出现的珠光体晶体学取向关系的类型并没有明显影响。

关键词：强磁场，相变，磁偶极子作用，织构，取向关系

Chapter 1 Literature Review

1.1 General introduction

The earliest known descriptions of magnets and their properties were around 2500 years ago, from Greece, India, and China, when man happened to notice the lodestones and their affinity to iron. Since then, people were undergoing a long period from being curious about its magnetic power, and attempting to uncover the physical essence, to fully understand it and even to establish corresponding theory to make use of it for every aspect of daily life and scientific researches.

Magnetic field is considered as a powerful tool for studying the properties of matter, because they couple directly to the electronic charge and magnetic moments of the protons, neutrons, and electrons of which matter is made up. In fact, all the matters are magnetic, but some materials are much more magnetic than the others. The origin of magnetism lies in the orbital and spin motions of electrons and the way by which the electrons interact with one another. The magnetic behavior of materials can be classified into five major groups: diamagnetism, paramagnetism, ferromagnetism, ferrimagnetism and antiferromagnetism (The ordering of magnetic moments in diamagnetism, paramagnetism, ferromagnetism, ferrimagnetism and antiferromagnetism materials have been shown in Figure 1.1). Diamagnetic substances are composed of atoms which have no net magnetic moments-all the orbital shells are filled and there are no unpaired electrons. Many everyday materials, e.g., water, wood, glass and many elements, e.g., H_2, Ar, Cu, Pb, are diamagnetic. When a diamagnetic material is exposed to an external field, it magnetized: a negative magnetization is produced. If the field is removed, the magnetization of diamagnetic material vanishes. For paramagnetic materials, some of the atoms or ions have a net magnetic moment due to unpaired electrons in

partially filled orbitals. The individual magnetic moments do not interact magnetically, so the total magnetization is zero without a field. In the presence of a field, there is a partial alignment of the atomic magnetic moments in the direction of the field, resulting in a net positive magnetization and positive susceptibility. In addition, the efficiency of the field in aligning the moments is opposed by the randomizing effects of thermal agitation. This results in a temperature dependent susceptibility, known as the Curie Law. Unlike paramagnetic materials, the atomic moments in ferromagnetic materials exhibit very strong interactions. These interactions are produced by electronic exchange forces and result in a parallel or anti-parallel alignment of atomic moments. Ferromagnetic materials exhibit parallel alignment of moments resulting in large net magnetization even in the absence of a magnetic field. Even though electronic exchange forces in ferromagnets are very large, thermal energy eventually overcomes the exchange and produces a randomizing effect. This occurs at a particular temperature called the Curie temperature (*Tc*). Below *Tc*, the ferromagnet is ordered and above it, disordered. The saturation magnetization goes to zero at the Curie temperature. For ferrimagnetic materials, the magnetic moments of the atoms on different sublattices are antiparallel. However, the opposing moments are unequal and a resolved spontaneous magnetization remains. If the opposing moments are exactly equal, the net moment is zero. This type of magnetic ordering is called antiferromagnetism.

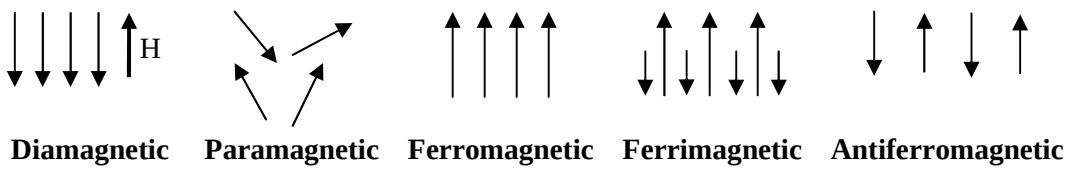

Figure 1.1 Magnetic ordering in magnetic materials.

Under the magnetic field, the field effect on different materials will be verified according to their magnetic behaviors, this underlie the essence of the magnetic field effect in material science.

As the development of the magnetic field theories and technique the application of the high magnetic field is greatly encouraged. High magnetic field as a clean, non-contacting and powerful source of energy can affect atomic behaviors, such as atom arrangement, matching and migration and thus exert powerful influence on microstructures and properties of materials. Consequently, more and more meaningful results and new phenomena together with economic profits are brought, which in turn inspires stronger desire to conduct more widening and deepening research.

Recently, magnetic field has been introduced to solid phase transformations of metallic materials; especially Fe-C based alloys, for the purpose of microstructure control. As is known, steels are the most widely used materials related to every industry in daily live. Any small improvement in properties of Fe-C alloys means a big progress in human being and a huge amount of interests. Together with a bright prospective based on mature knowledge, the study of phase transformation of Fe-C based alloys under high magnetic field has attracted special attention from all over the world, and will become a popular topic in the following years.

1.2 Basic mechanisms of the magnetic field influence on solid phase transformations in steels

Solid phase transformations in steels are often referred to the decomposition of austenite, which is usually classified into three groups: diffusionless, semi-diffusional and diffusional transformations, from a viewpoint of atom moment. The diffusionless phase transformation is known as martensitic transformation which occurs without long-range diffusion of neither Fe nor C atoms; semi-diffusional

transformation refers to the bainitic transformation, when only C atoms diffuses; as for diffusional transformation, it usually corresponds to the pearlitic and ferritic transformations, in which cases, both Fe and C atoms can fulfill a long-range diffusion. In terms of these solid phase transformations in steels, the phases involved are with different magnetisms. There are three equilibrium phases with great engineering importance located within different carbon composition and temperature range. One is high temperature austenite; the others are ferrite and cementite, which are considered as basic components to the product of the austenite decomposition. High temperature phase austenite is paramagnetic; ferrite is ferromagnetic below ~770°C and cementite is paramagnetic at the formation temperature but becomes ferromagnetic below ~210°C. Due to the natural magnetic difference of parent and product phases, the transformation process and the resultant microstructure could be modified by an external magnetic field. This is because that magnetic field could modify the energy terms due to its magnetization effect during the phase transformation and thus affect the phase transformation both thermodynamically and kinetically.

Take the phase transformation from austenite to ferrite for an example, when an external magnetic field was applied, the phases under the magnetic field will be magnetized and their Gibbs free energy will be changed by introducing so-called intrinsic magnetization energy. This magnetization energy is also denoted as the "magnetic Gibbs free energy", it can be written as $V\int_0^M \mu_0 H_0 dM$, where V is the volume of the phase, μ_0 the permeability of free space (vacuum), H_0 the magnetic field strength in free space and M the induced magnetization per unit volume. Therefore, for a transformation from austenite to ferrite in the presence of a magnetic field, the total Gibbs free energy change ${}^{M}\Delta G^{\gamma\to\alpha+\gamma}$ will contain two terms:

the "chemical Gibbs free energy difference" ΔG^C and the "magnetic Gibbs free energy difference" ΔG^M as follows:

$$^M\Delta G^{\gamma\to\alpha+\gamma} = \Delta G^C + \Delta G^M \tag{1.1}$$

$$\begin{aligned}\Delta G^M &= -(\int_0^{M^\alpha} Hd(\mu_0 M_\alpha) - \int_0^{M^\gamma} Hd(\mu_0 M_\gamma) \\ &= -H\mu_0(\int_0^{M^\alpha} dM_\alpha - \int_0^{M^\gamma} dM_\gamma)\end{aligned} \tag{1.2}$$

where superscript and subscript α and γ denote ferrite and austenite and M the magnetization. As the magnetization of ferrite is higher than that of austenite at all the transformation temperature concerned, ΔG^M has the same sign as ΔG^C. The absolute value of the Gibbs free energy difference between the two phases is increased. This leads to the new phase equilibrium and phase stability under the magnetic field by modifying the phase equilibrium temperature and equilibrium composition, as shown in Figure 1.2.

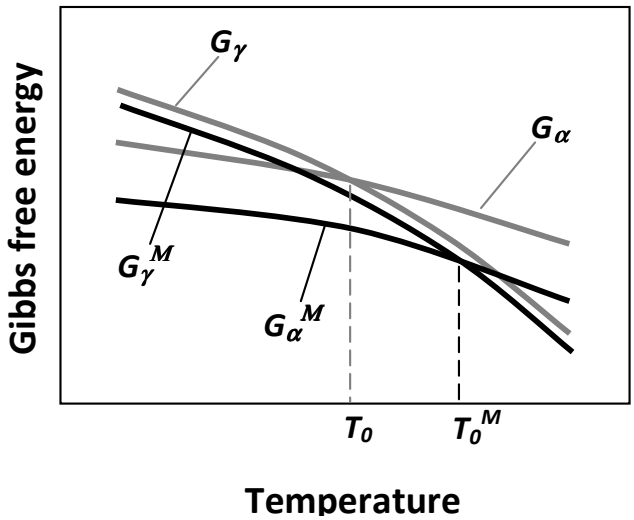

Figure 1.2 Schematics of the Gibbs free energy of γ and α without and with a magnetic field, γ-austenite, α-ferrite, M-magnetic field.

The Gibbs free energy difference between the parent and the product phases is also denoted as the phase transformation driving force which deal with the nucleation and growth process of the product phases, thus magnetic field affects not only the phase transformation thermodynamics but also the transformation kinetics such as modifying the transformation rate.

In addition to the thermodynamic and kinetic effects, there also exists magnetization and demagnetization effect of the magnetic field resulting from the strong magnetic interaction among the magnetic moments of Fe atoms when placed in a magnetic field. It is called magnetic dipolar interaction. Each Fe atom can be treated as a magnetic dipole. When an external magnetic field is applied, the atomic moments tend to align along the field direction, as schematized in Figure 1.3. Then, there exists the dipolar interaction between neighboring dipoles. They attract each other along the field direction (magnetization), but repel each other in the transverse field direction (demagnetization).

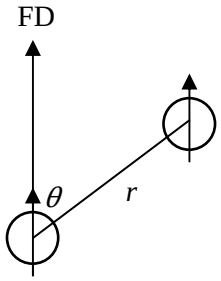

Figure 1.3 A pair of magnetic dipoles in a magnetic field.
FD: magnetic field direction.

This dipolar interaction has mainly microstructural effect as it works on the nucleation and the growth process of ferrite during the transformation from austenite to ferrite, especially when ferrite is ferromagnetic with high magnetization. By minimizing the demagnetization energy (repelling among magnetic moments), it

may bring about grain shape anisotropy by preferential grain growth in the field direction or crystallographic texture by selective grain nucleation or growth.

1.3 Solid phase transformations in steels under magnetic field

As mentioned above, since the magnetic natures of the parent and product phases involved in solid phase transformation in steels are usually different, the phase transformation process is expected to be modified by the application of magnetic field and the field influence is of great importance to be investigated.

In 1960's, studies on the effects of the magnetic field on austenitic decomposition began with the diffusionless martensitic transformation. As for martensitic transformation, the transformation temperature is relatively low and transformation can only be studied under low magnetic fields. As soon as the maturity of superconducting technique, the generation of direct current high magnetic field was available. From then on, a number of high temperature phase transformations under magnetic field are studied including semi-diffusional transformations and diffusional transformations. Although the studies on diffusional phase transformation under the magnetic field had a relatively late start, the results on this issue are far more fruitful than the other two.

1.3.1 Diffusionless transformation-Martensitic transformation

Martensitic transformation is the representative diffusionless transformation in ferrous alloys which involves austenite with face-centered-cubic crystal structure transforms to carbon oversaturated martensite with basically body-centered-cubic or body-centered-tetragonal crystal structure depending on carbon oversaturation degree. In martensitic transformation, the parent austenite is paramagnetic; whereas the martensite is ferromagnetic. The induced magnetization of martensite is much higher than that of austenite. When the magnetic field is applied, the Gibbs free energy of austenite does not change much but that of martensite is greatly lowered.

Thus, the phase equilibrium between parent and product phases is changed by magnetic field. For many years, the investigations on martensitic transformation under the magnetic field were focused on the effect of the magnetic field on increasing the *Ms* temperature and enhancing the amount of transformed martensite.

In early 1960's, studies on athermal martensitic transformation reported that magnetic field promoted martensitic transformation and increased the *Ms* temperature in ferrous alloys. Krivoglaz *et al.* [1] based on their thermodynamic analysis suggested that the effect of magnetic field on martensitic transformations be due only to the magnetostatic (Zeeman) energy. They proposed following formula to estimate the shift of *Ms*:

$$\delta T = \delta M \cdot H \cdot \delta V \cdot T_0 / q \tag{1.3}$$

where δM is the magnetization difference between the product and the parent phases, H the strength of applied magnetic field, δV volume change between the two phases and q the latent heat of transformation. The calculated shift of *Ms* for Fe-Ni alloys fitted well the experimental results [2, 3] .

Based on this, Kakeshita *et al.* [4-21] carried out more systematical and deeper studies on this issue. They used pulsed magnetic fields to induce larger increases in *Ms* and noticed that there existed a critical strength of magnetic field to effectively induce martensitic transformation at the temperatures above *Ms*, and the higher the temperature was, the stronger the critical strength became. They also found that the experimentally measured increases in *Ms* temperature of the Fe-Pt ordered and disordered alloys [5, 20], Fe-Ni-Co-Ti thermo-elastic alloys [7] and Fe-Ni alloys [6, 9] were not in agreement with the calculated results using Krivoglaz's formula (Eq. 1.3). They proposed a more accurate expression for the magnetic Gibbs free energy change by clarifying the unknown effects which Krivoglaz [1] did not find under

low field as the high field susceptibility and forced volume magnetostriction effects and gave the new estimation formula of the increase of *Ms* as follows [17]:

$$\Delta G(Ms) - \Delta G(Ms') = -\Delta M(Ms') \cdot H_c - (1/2) \cdot \chi_h^p \cdot H_c^2 + \varepsilon_0 \cdot (\partial w / \partial H) \cdot H_c \cdot B \quad (1.4)$$

in which $\Delta G(Ms)$ and $\Delta G(Ms')$ represent the difference in the Gibbs chemical free energy between the austenitic and martensitic phases at temperatures *Ms* and *Ms'* (*Ms'* the martensitic transformation start temperature under magnetic field) $\Delta M(Ms')$ the difference in spontaneous magnetization (magnetic moment) between the austenitic and martensitic states, *H* the strength of magnetic field, H_c the critical magnetic field to induce martensitic transformation, χ_h^p the high field susceptibility of the parent austenite, ε_0 the transformation strain, $(\partial w / \partial H)$ the forced volume magnetostriction and B the bulk modulus. The relations between $\Delta Ms (= Ms' - Ms)$ and H_C have been calculated for Fe-Pt alloys [5], Invar Fe-Ni [6], non-Invar Fe-Ni-C [8] and Invar Fe-Mn-C alloys [10], which are in good agreement with the experimental ones. The authors also clarified the influence of composition [6], grain boundaries [9], crystal orientations [8, 9], Invar characteristics [8], thermo-elastic nature [7, 20] and austenitic magnetism [14] on the magnetic field-induced martensitic transformations. Results showed that Eq. (1.4) suited well under the above conditions. Thus, the propriety of the newly derived equation is quantitatively verified.

As for the influence of the magnetic field on the kinetics of martensitic transformation, Kakeshita *et al.* [13, 14] conducted their investigation in Fe-Ni-Mn alloys. Their results suggest that, under high magnetic fields, the originally isothermal kinetics of martensitic transformation can be changed to the athermal one and the kinetics in both case can be evaluated from the same equation. They

also suggested [15] that the shift of the nose temperature and incubation time increase with increasing magnetic field.

The martensitic morphologies under the magnetic field have also been studied in a variety of Fe-based alloys. Many studies showed that the structure of the magnetic field-induced martensite did not show much difference [4-21]; whereas the amount of martensite was increased by the magnetic field [6, 12]. The increase in the amount of martensite is very meaningful and important, as it will result in further strengthening, considering that martensite is a hard phase, whereas austenite is a soft phase.

1.3.2 Semi-diffusional transformation-Bainitic transformation

The study on the effects of magnetic field on bainitic transformation has a relatively late start, and only a few researches have been done. In this case, the parent austenite is paramagnetic and the product bainite is ferromagnetic like martensite. In this content, the effect of magnetic field on bainitic transformation is similar to the case of martensitic transformation, on both thermodynamic and kinetic aspects.

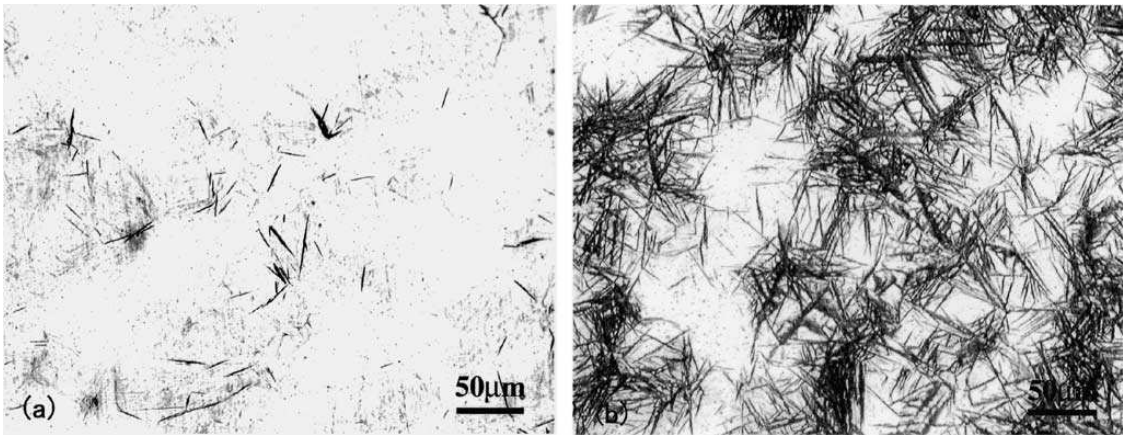

Figure 1.4 A Fe-0.52C-0.24Si-0.84Mn-1.76Ni-1.27Cr-0.35Mo-0.13V (mass) alloy austenitized at 1000°C and transformed isothermally to bainite, followed by helium quenching to ambient temperature. (a) 0T and (b) 10T [23].

Grishin [22] made an investigation on the transformation from austenite to bainite under a magnetic field based on three different structural steels. It revealed that the bainitic transformation was accelerated by magnetic field. The acceleration effect by field was also observed in Fe-0.52C-0.24Si-0.84Mn-1.76Ni-1.27Cr-0.35Mo-0.13V alloy by microstructural observation. As shown in Figure 1.4 [23], the amount of the transformed bainite (black) was greatly increased under the 10T magnetic field.

Later, effects of magnetic fields on transformation temperature, transformation behavior and transformed microstructure have been investigated for bainitic transformation in a Fe-3.6Ni-1.45Cr-0.5C steel [24, 25]. It was found that the *Bs* temperatures increase with the increase of the applied magnetic field. Bainitic transformation is accelerated by the applied magnetic field.

Although elongated and aligned microstructures were observed for austenite to ferrite transformation in a Fe-0.4C alloy, but no elongation or alignment of transformed structure has been observed for transformations to bainite and lath martensite.

1.3.3 Diffusion-controlled phase transformations under magnetic field

Compared with diffusionless and semi-diffusional transformation, the diffusion-controlled phase transformations in steels are more complicated and intricate, due to the variety of the proeutectoid phases diversified by carbon composition. As the diffusional phase transformations usually happen in relatively high temperature range, experimental studies are difficult to conduct, especially when high magnetic field is difficult to be obtained. Studies on this subject began from the theoretical simulation calculations instead. Only until 1980's, magnetic field was tried to be applied to the diffusion-controlled transformation. Later, with the development of magnetic field technology, more experiments on diffusion-controlled transformations under magnetic field have been carried out in various Fe based alloys under the instruction of the calculated results. Since then, more and

more new phenomena have been uncovered and verified. In the meantime, corresponding theories have been explored for better understanding of magnetic field influential mechanisms. Unlike the martensitic transformation and bainitic transformation, in which the magnetic field effects were largely from energy aspects and work on the transformation thermodynamic and kinetic, but less on morphology, the influence of magnetic field on diffusional phase transformation were more widely and complicated, which also involved with the magnetic dipolar interaction and thus leads to the effects from both crystallographic and morphologic point of view.

1.3.3.1 New Fe-C phase equilibrium under the magnetic field

When people tried to understand the Fe-C solid phase transformation under magnetic field, they started from understanding the field effects on phase equilibriums. Even in earlier days, when experimental studies on the effects of magnetic field on diffusion-controlled solid phase transformation in steel were not available, thermodynamic calculations were carried out to explore field effects, and later the calculation results were applied to guide the experimental studies.

The influence of magnetic field on phase equilibrium first expressed as the shift of phase transformation temperature. In 1965, Sadovskii *et al.* [26] mentioned that with the increasing intensity of the magnetic field, the amount of the magnetic phase formed increases and the range of the existence of the phase increases with the degree of magnetization in a way similar to the effect of pressure. It was pointed out that the change in the temperature of the phase transformation under the influence of the magnetic field is expressed by the equation:

$$dT/dH = \Delta J T_0/q \tag{1.5}$$

where H is the intensity of the field; ΔJ is the difference in the magnetization of the phase intervening in the transformation; T_0 is the temperature of phase equilibrium;

q is the heat of transformation. Later, Ghosh *et al.* [27] investigated the change of TTT diagram using a similar equation during austenite to ferrite transformation. This analysis did not take the magnetization of austenite into account, thus, it is only suitable for low magnetic field. When magnetic field is strong, the ignorance of the magnetization of austenite was quite a deviation from real situation, let alone the influence brought by composition changes. Although the equation is useful in a limited range, it is a very instructive calculation of the effects of magnetic field on solid phase equilibrium of iron based alloys.

The studies of phase diagram are meaningful and necessary due to its guiding role in designing heat treatment plan and developing new materials. The basic idea of building up a new Fe-C phase diagram is to determine the new phase equilibrium temperature and equilibrium composition under the external magnetic field. In terms of this, the change of the Gibbs free energy induced by the magnetic field of related phases has to be evaluated by using appropriate mode and magnetic parameters.

From last 90’s, studies on the Fe-C phase diagram under the field have been launched by researchers from Korea and Japan. Considering that the absence of high-field magnetic susceptibility data around *Tc* makes it impossible to construct the Fe-C phase diagram under the high magnetic field based on the experimental data, they used the molecular field theory, which is capable to provide a theoretical method to estimate the high-field magnetization in this temperature region. As a result, former studies were based on the Weiss molecular field theory together with the Curie-Weiss law to evaluate the change in Gibbs free energy of individual phases involved with the applied magnetic field.

Meanwhile, experimental measurements are important and needed to verify the validation of the calculated results. In term of this, experimental measurements of

phase transformation temperature and examination on transformed microstructure had been made as powerful and direct methods to offer comparative study.

The first comprehensive study on the prediction of the new Fe-C phase diagram under the magnetic field was carried out by Joo *et al* [28]. Considering the disagreement of magnetic susceptibility of ferrite from Curie-Weiss law and experimental data, the magnetization calculated by Weiss theory is used instead of susceptibility to calculate the magnetic Gibbs free energy of ferrite. In this work, the influence of the magnetic field on all phases was concerned, the Fe-C phase diagram were calculated under various applied magnetic fields and the eutectoid temperature, eutectoid composition as well as the γ/α transformation temperature were determined. Results showed that both Ac_1 and Ac_3 temperatures increase as the magnetic field is applied, while the Ac_m temperature change is almost independent of the field. As a result, eutectoid point was shifted to high carbon and high temperature side, as seen in Figure 1.5.

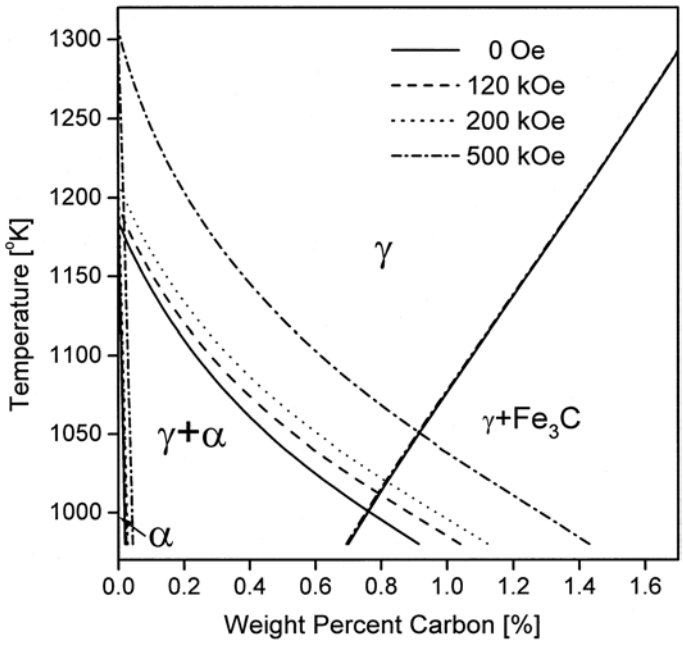

Figure 1.5 Fe-C phase diagram associated with the $\alpha/\gamma+\alpha$, γ/α and γ/Fe_3C equilibrium transformation for various applied magnetic fields [28].

It is regarded for the first time the simulation of the Fe-C phase diagram under the field. This study is quite limited, because the magnetic Gibbs free energy of ferrite is obtained by mathematic method without interpreting the inner physic relation between *M*, *H* and *T*. Moreover, the prediction of the magnetic Gibbs free energy at any field strength is not obtainable. This limits the application of this study to some extent. Despite of this, the results obtained from this work are of great importance and meaning. It showed that the applied magnetic field could affect the phase equilibrium temperature as well as the eutectoid composition, and thus change the microstructure at room temperature. This enables the application of magnetic field as a method of microstructure control and materials properties optimization. In addition, the shift of eutectoid point by magnetic field enables the possibility of improving mechanical properties by increasing carbon content without hypereutectoid transformation. Joo *et al.* [29] measured the γ-α transformation temperature under 10T magnetic field by thermo-dilatometer. It turned out that the increase of the γ-α transformation temperature in pure iron and the eutectoid temperature calculated on the basis of molecular field theory are in good agreement with measured results [28].

Similar calculations using Weiss molecular field theory to calculate Gibbs free energy change of the phases were also carried out by Choi *et al.* [30], Guo and Enomoto [31, 32] as well as Hao and Ohtsuka [24, 25, 33-38] in Fe-C system.

Choi *et al.* [30] combined the calculation studies with experimental examination and proved that magnetic field can also increase the carbon content in eutectoid composition and solubility in ferrite. Guo and Enomoto even further enlarged their studies to Fe-C-Mn and Fe-C-Si alloys [31, 32] by taking into account the interaction free energy of the alloying elements as well as the influence of the alloying elements on Curie temperature and the magnetic moments of the iron atoms. Considering the Curie-Weiss law can hardly offer reliable susceptibility data

of ferrite around Curie temperature, these calculations were very approximate around and above the Curie temperature. However, valuable results were obtained that the α-γ transformation temperature is raised 1-3°C per Tesla depending on the alloy composition and the intensity of the applied field, whereas the γ-δ transformation temperature is decreased about 0.4°C per Tesla. They also predicted that, at about 100T pure *bcc* iron may be more stable than the *fcc* iron at all temperature range. Hao and Ohtsuka [33] revealed that: It was found that when magnetic field is lower than 10T, the transformation temperature for pure Fe from austenite to ferrite has a linear relationship with magnetic field strength, increasing about 0.8°C per Tesla. For eutectoid transformation in Fe-0.8C alloy, similar relationship exists, the transformation temperature increases about 1.5°C per Tesla. Hao and Ohtsuka [33] used the thermocouple and a digital recorder to measure the transformation temperature. It was indicated that the measured transformation temperature data are not consistent with calculation results using Weiss molecular field theory and moreover, using the experimental measured susceptibility under a low magnetic field to conduct the simulation calculations for high magnetic field is not appropriate.

It was noted that Weiss model allows basic calculations for ferromagnetism and offers relatively accurate magnetization data of *bcc* Fe below *Tc*, however, it still had several shortcomings [32], which limited the application of Weiss model around and above *Tc*, especially when the applied magnetic field is high. Thus, new models were needed for simulation calculation of Fe-C equilibrium under the magnetic field.

To solve this problem, Zhang [39] revised the Weiss model by substituting the molecular field coefficient λ with a short-range-ordering coefficient γ around and above *Tc* and applied this revised mode to the susceptibility of *bcc* Fe above *Tc*, which turned out to be in good agreement with the ones measured experimentally.

Moreover, the electronic band model is used to calculate the temperature variation of susceptibility of *fcc* Fe. Based on these, the magnetization and further the magnetic Gibbs free energy of ferrite and austenite are calculated, thus the Fe-C phase diagram under the magnetic field was calculated, the shift of Ae_3 temperature and the eutectoid temperature and composition are predicted. It is found that in the phase diagram the magnetic field enlarges the ferritic phase area and shrinks the austenitic one. With pure iron, the Ae_3 is raised by about 7°C under a magnetic field of 10T. This result is in good agreement with the measured values by Ohtsuka *et al.* [33].

Generally, for Fe and Fe-0.8C the average γ-α transformation temperature measured experimentally was easily compared with the calculated results based on Weiss molecular field theory. The most accepted result was that the change of γ-α transformation temperature is almost proportional to the magnetic field when the ferrite phase is ferromagnetic at the transformation temperature (as is the case in Fe-0.8C), whereas it was proportional to the square of the magnetic field when the ferrite phase is paramagnetic (as is the case in pure iron). However, for intermediate pro-eutectoid steel, of which the (γ+α) region is large, this method is no longer valid [40] and it would have been meaningless to define an average γ/α transformation temperature in order to compare it with a calculated γ/α equilibrium temperature due to the large hysteresis of the transformations in these alloys. Considering this, another approach was proposed to discuss the magnetic field dependence of diffusional phase transformation temperatures, taking into account the existence of temperature hysteresis due to the large driving force required for transformation [41]. More recently, this new approach was applied to study the non-equilibrium α-γ and γ-α transformation temperature separately in Fe-Rh alloys [41], Fe-C-Mn alloys [42] and Fe–Ni alloys [43, 44].

Together with the development of new analysis approach, new devices to monitor high temperature phase transformations under magnetic field had emerged. Rivoirard and Garcin [42, 45, 46] developed a high magnetic field in situ dilatometer, ranging from room temperature up to 1500K, using a high resolution Michelson laser interferometer. This new devices were applied to monitor the austenite to ferrite transformation under a magnetic field of 16T in pure iron. Then, measured Ar_3 temperatures were compared with the calculated results. In their studies, experimental magnetization data, measured up to 3.5 T and 1100 K by high-sensitivity magnetometer [47], were used to calculate the magnetic contribution to the Gibbs free energy instead of the calculated one from Weiss molecular field theory. In this approach, calculated Ar_3 temperatures were found to be in good agreement with the experimental ones measured by dilatometer.

Besides the modification of γ-α transformation temperature, the eutectoid point shift has also been calculated and experimentally evidenced in hypereutectoid carbon steel [48, 49]. Microstructural observation, which indicates formation of ferrite in the hypereutectoid carbon steel under field, evidences the shift of the eutectoid point in the Fe-C system. It shifts under a 12 T magnetic field from 0.77 wt. %C to 0.8287 wt. %C.

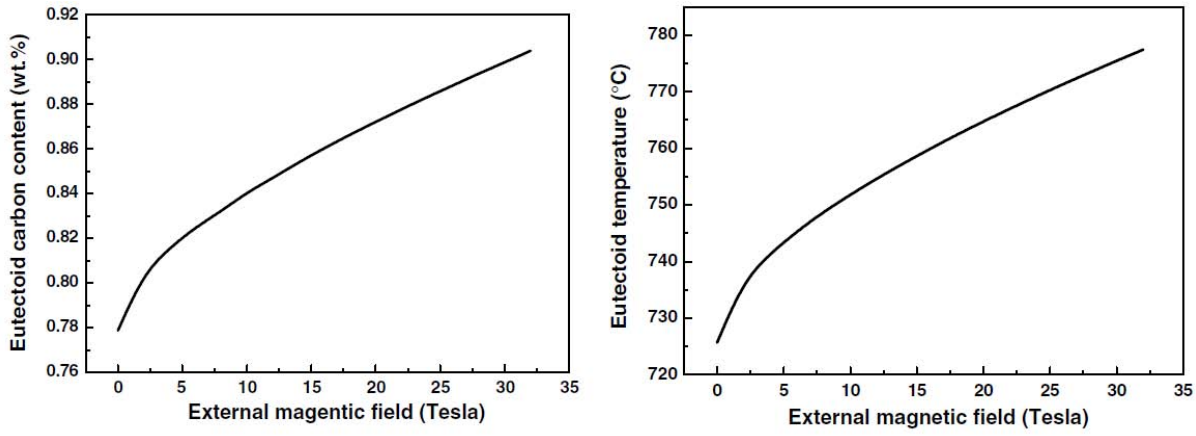

Figure 1.6 Eutectoid carbon content and temperature as a function of the magnetic field induction [49].

Furthermore, Zhang *et al.* [48, 49] propose a general and comprehensive calculation method by combining the well-established statistical thermodynamic models with the magnetism theory to predict this eutectoid point shift (both in carbon composition and temperature scales) as shown in Figure 1.6.

The eutectoid carbon content and temperature calculated without and with a 12 T magnetic field is 0.779 wt. %C; 725.71 °C and 0.847 wt. %C; 754.68 °C. The eutectoid carbon contents without and with the magnetic field-as calculated-appears to be very close to the values determined experimentally. It shows that the equations proposed offer a relatively accurate prediction of the eutectoid point shift under a high magnetic field in both carbon content and temperature scales.

1.3.3.2 New microstructural features under the magnetic field

The most remarkable microstructural feature induced by magnetic field is the formation of the aligned and elongated microstructures during transformation between austenite and ferrite. Studies on this subject have been drawing increasing attention as it may lead to the control of the microstructure and thus the texture and the mechanical properties.

The first observation of the aligned microstructure was reported by Shimotomai [50] in Fe-0.1C alloy and Fe-0.6C alloy during the α to γ inverse transformation. The chains or columns of the paramagnetic austenite were found along the field direction in the ferromagnetic ferrite phase during the ferrite to austenite inverse transformation in 8T magnetic field, as shown in Figure 1.7.

They contributed the formation of the alignment to the dipolar interactions of the magnetic moments between the pairs of paramagnetic austenite nuclei which are regarded as magnetic hole in ferrite matrix. Later, the alignment of the γ nuclei under the field effect was even noticed above the Curie temperature during γ-α inverse transformation [51].

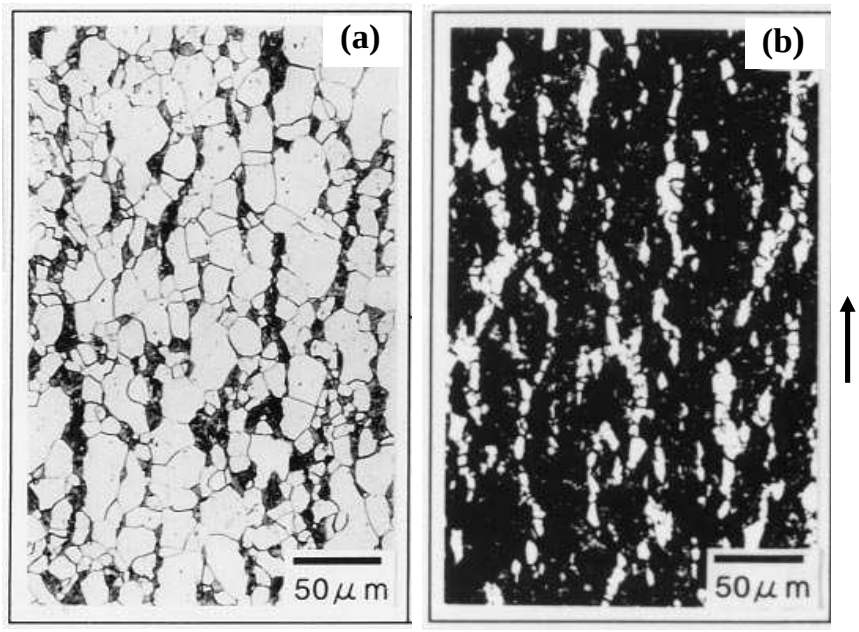

Figure 1.7 Microstructures of Fe-0.1C alloy (a) and Fe-0.6C alloy (b) subjected to the α/γ inverse transformation under 8T magnetic field [50]. (The dark spots are γ phase followed by quenching to a new martensite, while the light regions represent the annealed α phase-initial martensitethe. The arrow indicates the direction of the magnetic field).

Later, Shimotomai and Maruta studied the magnetic field-induced alignment structures in Fe-0.6C alloy, Fe-0.2C-0.2Si-1.3Mn-0.1Ti alloy and Fe-0.1C-2.0Si-2.0Mn [51-53] during the γ-α transformation. A special experimental setup was designed, which features a combination of roller dice for hot deformation and a superconducting magnet for applying a magnetic field during the phase transformation. The concept is characterized by deforming steels prior to the transformation under the field in order to introduce more nucleation sites for transformation. In their studies, the formation mechanism of the aligned structures has been discussed from the point of view of nucleation and growth of the ferrite grains. They observed the ferrite nucleation sites under the field using SEM and drew a conclusion that no matter the nucleation site is at the grain boundary or in the austenite grain interiors, the long axis of the ferrite grain is always parallel to the field direction, as shown in Figure 1.8. Further analysis on ferrite morphology

showed that the ferrite particles nucleated and grew along the magnetic field direction are mostly ellipsoidal in shape and this is determined by a competition between the magnetic field energy that favors an elongated shape and the interfacial energy that favors a spherical shape. Moreover, it was reported that, though ferrite grains were elongated and aligned by applied field, no preferred crystallographic orientation of ferrite is developed.

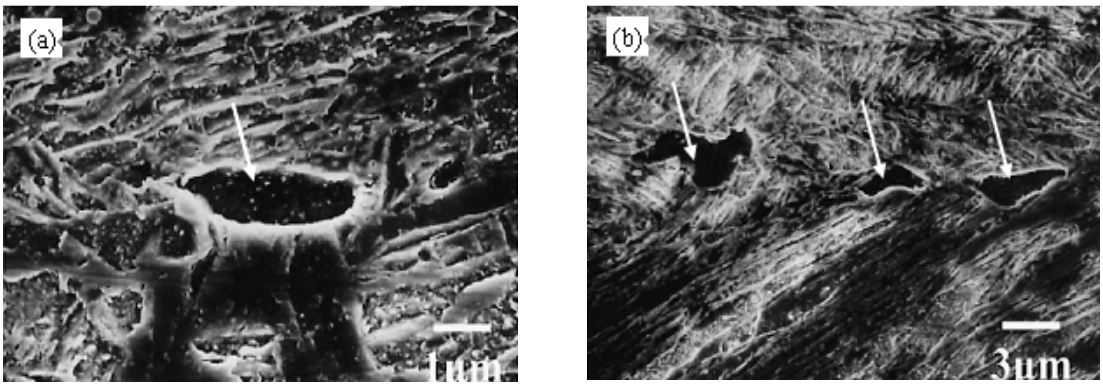

Figure 1.8 SEM micrographs of Fe-0.1C alloy under 12T magnetic field
(a) a ferrite particle nucleated inside an austenite grain,
(b) ferrite particles nucleated at the grain boundary of austenite.

Shimotomai and Maruta considered a combination of prior rolling and transformation in an external field is essential for yielding an aligned structure during γ-α transformation. However, a similar aligned structures were reported by Ohtsuka *et al* in a Fe-0.4C alloy without prior deformation during continuous slow cooling under the 10T magnetic field [36]. As seen from Figure 1.9, each ferrite grain is elongated and these grains are distributed head to tail along the field direction.

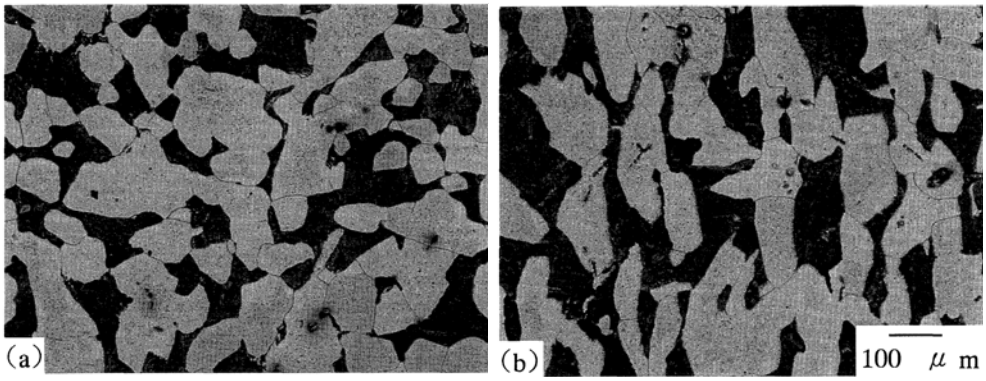

Figure 1.9 Microstructures of Fe-0.4C alloy during continuous slow cooling from γ to α transformation under 10T magnetic field (The field direction is vertical) [36].

Later, Hao and Ohtsuka [34, 35, 37, 54] studies the effect of magnetic field on transformed structure for γ to α isothermal transformation in Fe-C alloys to clarify the mechanism of the elongation and alignment of ferrite grains. They found that during the isothermal transformation, the elongated and aligned structure is mostly formed during grain growth rather than nucleation. The degree of elongation of ferrite grains is determined by the competition between the demagnetization effect and the chemical driving force and their combined effects result in the degree of elongation reaching a peak value at approximately *Tc*. The degree of elongation of ferrite grains as a function of isothermal holding time and temperature in a magnetic field of 10T in Fe–0.4C were shown in Figure1.10.

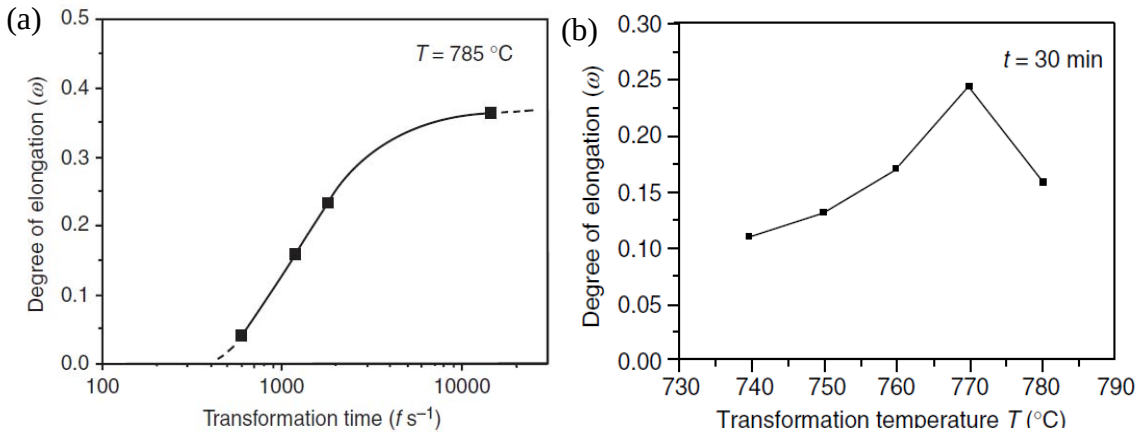

Figure 1.10 The degree of elongation of ferrite grains as a function of isothermal holding time and temperature in a magnetic field of 10T in Fe–0.4C alloy [35].

The effects of magnetic field strength, cooling rate and austenite grain size on the transformed structure in a magnetic field were observed for Fe-Mn-C-Nb alloy, but no elongation or alignment of ferrite grains has been observed [36]. On this basis, the existence of alloying elements may totally eliminate this elongation and alignment morphology.

Later, Zhang *et.al* [55-57] found that the aligned structure formed during slow cooling process rather than fast cooling process, when they studied the austenite decomposition in a hot-rolled 42CrMo steel under the magnetic field. They suggested that when cooling rate is 10°C/min, due to the inhomogeneous deformation during rolling and the dipolar attraction between ferrite nuclei, the microstructure of alternately distributed ferrite grains and pearlite colonies along the field direction is obtained.

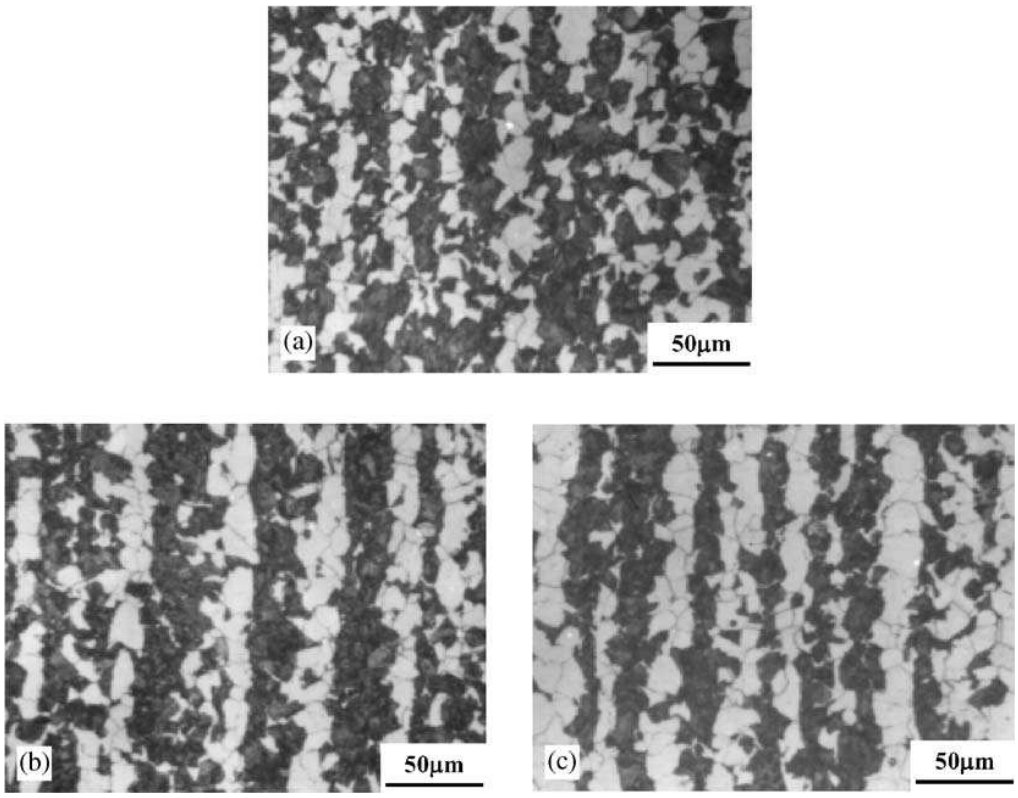

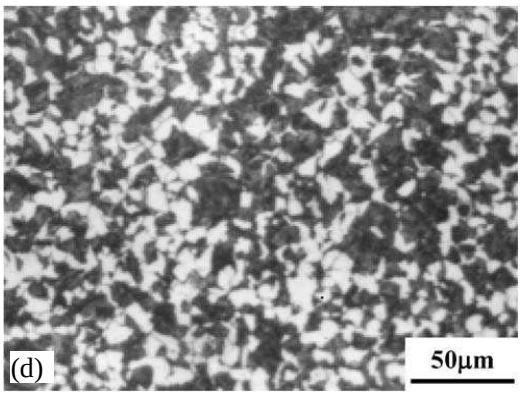

Figure 1.11 Microstructures after heating at 880°C for 33 min and cooling at 10°C /min with magnetic field of (a) 6T, (b) 10T, (c) 14T and (d) cooling at 46°C /min with 14T magnetic field.(the magnetic field direction and the rolling direction are vertical in the pictures) [56].

In the case of cooling at 46°C/min, the nucleation at high temperature is greatly inhibited; as a result, the nucleation is postponed at lower temperature, when more sites inside the austenite grains besides grain boundaries are available. Consequently, the microstructure is characteristic of randomly distributed ferrite grains and pearlite colonies with smaller sizes, seen in Figure 1.11.

The magnetic field-induced grain elongation mechanism was analyzed from physical point of view [58]. It revealed that the grain elongation is the results of the opposing contributions from the atomic dipolar interaction energy of Fe atoms and the interfacial energy.

The effect of magnetic field on the formation of elongated and aligned pearlite was investigated by Song *et al* [59]. It was reported that in the Fe-0.12C alloy, the pearlite was elongated and aligned along the field direction during its diffusional decomposition under the 12T magnetic field. Moreover, this tendency increased with increasing magnetic field strength and this field effect is dependent on the specimen orientation with respect to the field direction.

It should be noticed that, several works indicates that the nucleation and growth of ferrite grains happen preferentially along the field direction, however, no

preferred crystallographic orientations in the microstructure were formed [36, 50-53, 55-57].

Recently, magnetic field-induced microstructures features were investigated from crystallographic point of view. Zhang *et al.* applied a 12T magnetic field to a medium plain carbon steel during the diffusional decomposition of austenite and investigated the effect of a high magnetic field on the distribution of misorientation angles, grain boundary characteristics and texture formation in the ferrite produced [60]. It was reported that magnetic field can cause a considerable decrease in the frequency of low-angle misorientation and an increase in the occurrence of low Σ coincidence boundaries, especially the Σ3 of ferrite [60]. They attributed this to the elevation in the transformation temperature caused by the magnetic field and, therefore, the reduction of the transformation stress. It is also found that magnetic field enhances the <001> texture component along the transverse field direction due to the dipolar interaction between the magnetic moments of Fe atoms.

1.4 Significance and content of this work

The investigations on phase transformation under the magnetic field have been carried out for more than fifty years. Many meaningful experimental phenomena have been discovered and some related theories have been developed. Nowadays, as a new promising technique, magnetic field has been widely applied in materials processing. However, most of the former studies on the effect of the magnetic field on diffusional phase transformation are lack of regularity, and are not systematic either. The fundamental theories of magnetic field influence on phase transformation are still in need to be addressed. As alloying elements affect the phase transformation in steels to a large extent, the fundamental theories on field influential mechanism are hard to establish based on the existing studies, most of which were conducted in Fe-based alloys with considerable alloying elements. With

the development of the magnetic field generator technique, the application of magnetic field becomes more and more extensive. Deeper understanding of field influential mechanism is necessary and imperative. Based on such background, the present work has been carried out as a fundamental research to explore the magnetic field influential mechanism on diffusional phase transformation and also enrich the existing phase transformation theory. To examine the field effect without the involvement of impurities and alloying elements and to obtain a systematic result, three high purity Fe-C alloys in both hypo and hyper eutectoid composition range were prepared as experimental materials. The field induced microstructural features and the crystallographic characteristics have been thoroughly investigated. The main content of present work can be summed up as follows:

(1) Experimentally examine the microstructural features induced by magnetic field in both hypo and hyper eutectoid Fe-C alloys:

Magnetic field induced aligned and elongated microstructures are analyzed through a comparative study in Fe-0.12C alloy and Fe-0.36C alloy.

Microstructural modifications by magnetic field due to its thermodynamic influence on phase equilibrium in hypo and hyper eutectoid Fe-C alloys, respectively.

(2) Experimentally examine the modification of carbon solubility in ferrite under the magnetic field, conduct calculations on magnetic moments of the related atoms and underline the physical essence of the field influential mechanism using magnetic field dipolar interaction.

(3) By means of SEM/EBSD to examine the effect of the magnetic field on crystallographic orientation characteristics. The field induced preferred orientation distribution of ferrite and then the texture formation mechanism is investigated. The types of the orientation relationships in pearlite and the corresponding occurrence frequency have been examined.

Chapter 2 Experimentals and Calculations

2.1 Materials preparation

The materials used in this work are three high purity Fe-C alloys with different carbon content, namely, Fe-0.12C alloy, Fe-0.36C alloy and Fe-1.1C alloy. To minimize the involvement of impurities during the preparation, the alloys were prepared by vacuum induction melting using high purity constituent elements in EPM laboratory of Northeastern University, China.

The preparation of the high purity Fe-C alloys involves following two steps.

(1) Preparation of high purity cast iron as high carbon-content constituent for carbon content tuning of the alloys.

The high purity (99.99%) electrolytic iron was melted in a high purity graphite crucible (carbon 99.99%) by repeated vacuum induction melting, allowing carbon to diffusion into the iron melt from the graphite to produce cast iron. The chemical composition of the obtained cast iron is shown in Table 2.1.

Table 2.1 Chemical composition of cast iron, %.

C	S	O	N	Fe
4.39	0.001	0.0025	0.0003	Bal.

(2) Preparation of the final alloys with assigned carbon content.

The cast iron obtained in step (1) as high carbon constituent was melted with high purity (99.99%) electrolytic iron in water cooled copper crucible by vacuum induction levitation melting. By varying the quantity of the cast iron, the final Fe-C alloys with assigned carbon contents (0.12C, 0.36C and 1.1C in wt.%) were obtained. Figure 2.1 shows the top view of one high purity Fe-C alloy ingot.

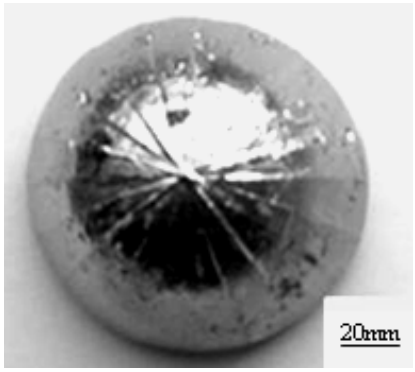

Figure 2.1 Photo of the ingot of the Fe-C alloy.

2.2 Pre-treatment of high purity Fe-C alloys

In order to study the influence of the magnetic field on phase transformation without the interference from the inhomogeneity of the initial microstructure, the three high purity alloys were pre-treated to obtain the homogeneous and equilibrium microstructures for the subsequent magnetic field heat treatments.

First, the ingots were multidirectionally forged to homogenize the microstructure. The multidirectional forging was performed by first forging the ingots into cubes and then further forging the cubes along their three perpendicular edge directions to resume the initial cube form of the work pieces. This process was repeated 4 times. Finally the cube was forged along one of its diagonal direction into a pancake shape. The multidirectional forging was conducted within the temperature range from 1273K to 1073K without annealing between the forging steps. After forging, the work pieces were air cooled to the room temperature. To avoid the involvement of the outside oxide coating and decarburized layer in the specimens, a plate of 70mm×70mm×35mm in size was cut out from the centre of each forged pancake by electrical spark cutting.

Then, the plates were homogeneously annealed in vacuum at set temperature for 10 hours to homogenize the composition. (The annealing temperature is 1373K for Fe-0.12C alloy and Fe-0.36C alloy; 1323K for Fe-1.1C alloy).

After that, full annealing was performed to obtain equilibrium microstructures. The alloys were fully austenitized for 45min, and cooled to 973K at 0.3K/min for proeutectoid and eutectoid transformation, and then cooled to room temperature at 1K/min (The austenitization temperatures for the full annealings are 1165K for Fe-0.12C alloy, 1099K for Fe-0.36C alloy and 1063K for Fe-1.1C alloy). The chemical composition of the high purity Fe-C alloys was analyzed using Carbon/Sulfur analyzer, Inductively Coupled Plasma spectrometer and Nitrogen/Oxygen exterminator, the result is shown in Table 2.2.

Table 2.2 Chemical composition of Fe-C alloys (wt.%).

C	S	P	Mn	Cu	O	N	Fe
0.12	0.0008	0.0006	＜0.001	0.001	0.0007	0.0003	Bal.
0.36	0.0008	0.0006	＜0.001	0.001	0.0007	0.0003	Bal.
1.1	0.0008	0.0006	＜0.001	0.001	0.0007	0.0003	Bal.

The corresponding phase equilibrium temperatures of the three alloys were calculated with Thermo-Calc Software. For the Fe-0.12C alloy and the Fe-0.36C alloy, their Ae_3 temperatures are 1135K and 1069K, respectively; for the Fe-1.1C alloy, Ae_{cm} temperature is 1128K.

2.3 Magnetic field heat treatment equipment and experiments

In this work, all the field heat treatments were conducted at EPM laboratory of Northeastern University, China. The magnetic field heat treatment furnace is set in a

12T cryo-cooled superconducting magnets with a bore sized 100mm in diameter (Figure 2.2 shows the photo (a) and the schema (b) of the magnetic field heat treatment furnace). The magnetic field ramping time from 0T to 12T is 39 minutes. For this magnetic field heat treatment furnace, the highest heating temperature is 1473K, the maximum heating rate is 5K/min and the maximum cooling rate is 23.5K/min. During the heat treatment, the vacuum degree in the heat treatment furnace can reach 10^{-3}Pa.

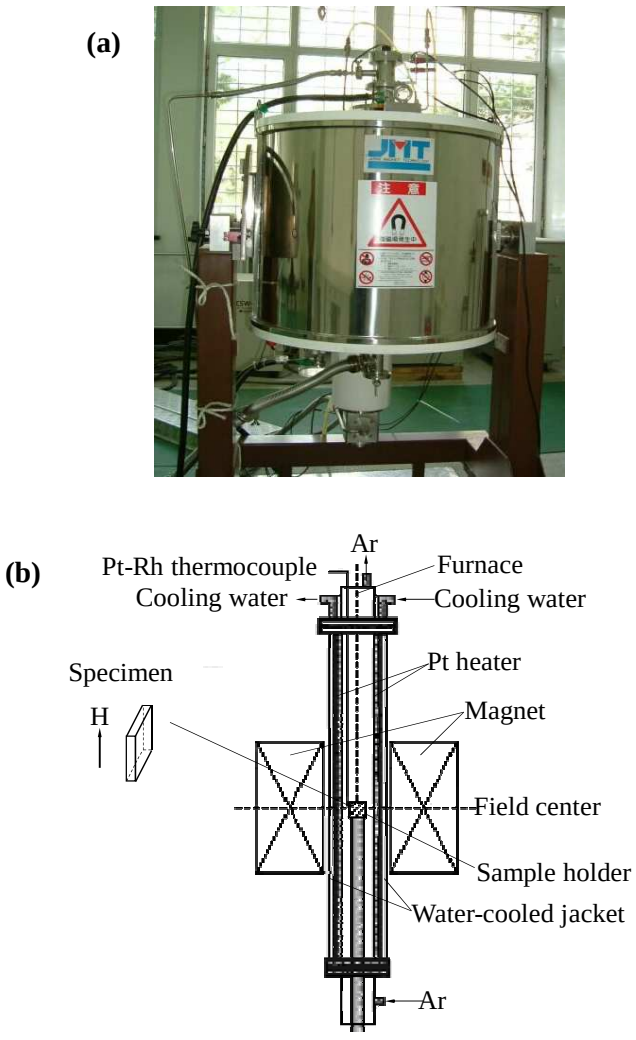

Figure 2.2 Photo (a) and schema (b) of magnetic field heat treatment furnace.

For field heat treatments, the magnetic field was applied during the whole heating, isothermal holding and cooling process. For Fe-0.12C and Fe-1.1C alloys,

the 12T magnetic field was applied, while for Fe-0.36C alloy, both 8T and 12T magnetic fields were applied. The non-field heat treatments for comparison were carried out in the same furnace using the same heat treatment parameters only without switching on the magnetic field. During the field heat treatment, the specimens were kept in the centre (zero magnetic force) area with one of their length directions parallel to the field direction, as shown in Figure 2.2(b). The detailed heat treatment parameters used in this work for the three alloys are illustrated in Figure 2.3. In the figures, the respective Ae_3 and Ae_{cm} temperatures of the three alloys are from the Thermo-Calc calculations but the Ae_1 temperatures are from the common accepted theoretical value (1000K).

(a)

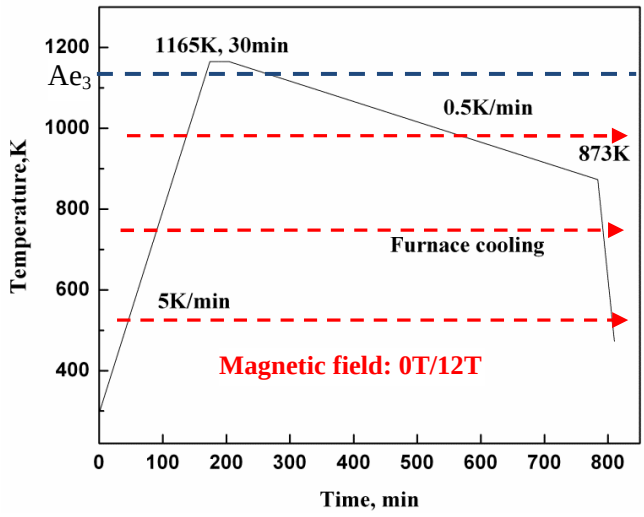

(b)

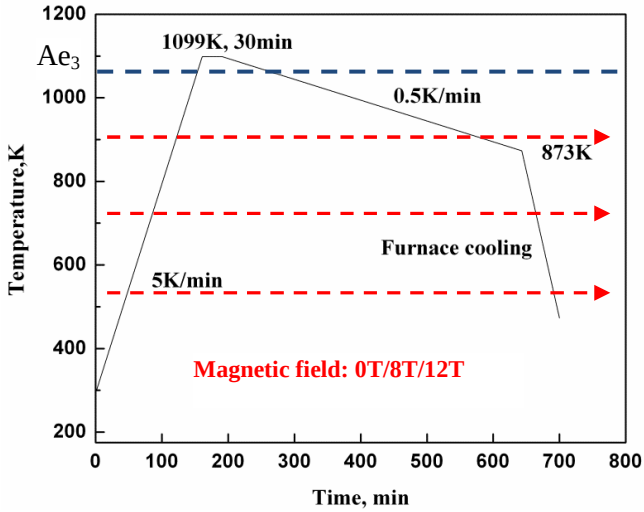

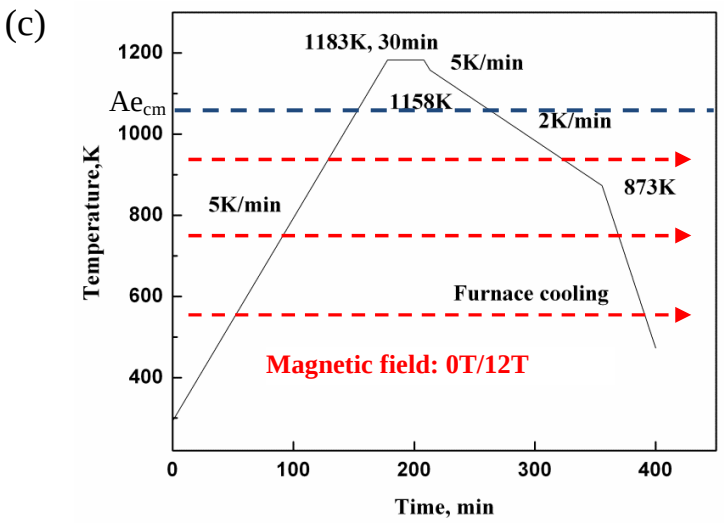

Figure 2.3 Heat treatment parameters for Fe-C alloys (a) Fe-0.12C (b) Fe-0.36C and (c) Fe-1.1 C. The respective Ae_3 and Ae_{cm} temperatures are calculated by Thermo-Calc, but the Ae_1 temperatures are from the common accepted theoretical value (1000K).

2.4 Specimen cutting and specimen geometry

For the final heat treatments, small sized specimens were cut out from the center of the plates after the pre-heat treatment. The dimensions of the specimens are 7mm×7mm×1mm for the Fe-0.12C alloy and the Fe-0.36C alloy; and 10mm×10mm×3mm for the Fe-1.1C alloy, as illustrated in Figure 2.4.

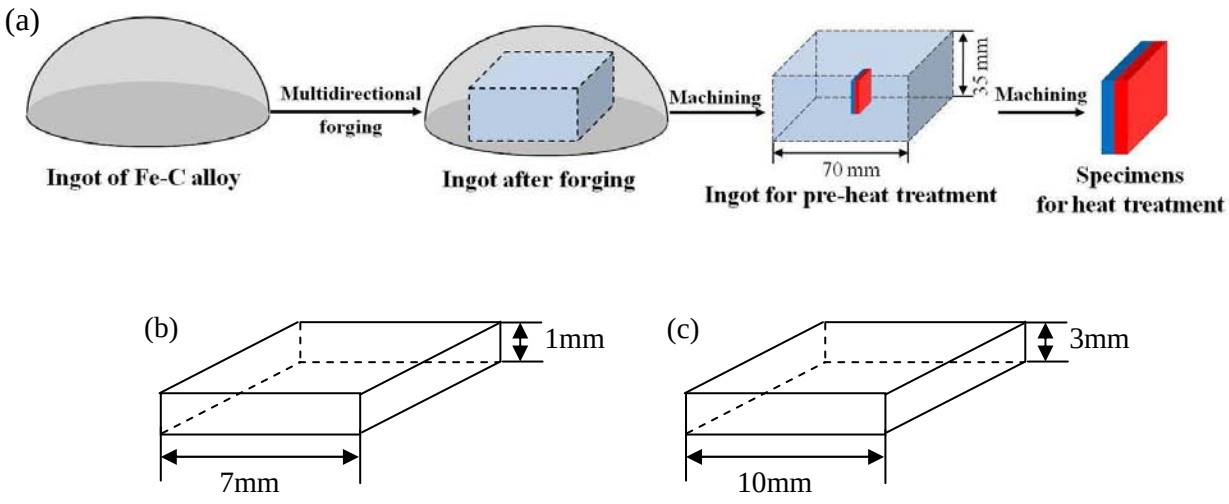

Figure 2.4 Illustration of specimens for heat treatments (a) and the sizes of the specimens (b) for Fe-0.12C alloy and Fe-0.36C alloy; (c) for Fe-1.1C alloy.

2.5 Microstructure examinations and crystallographic characterizations

2.5.1 Specimen polishing

To obtain an appropriate observation surface for microstructural examinations, the treated specimens were first mechanically polished using SiC grinding papers from 800# to 2000# and then polished using diamond liquid with the size of the diamond particle from 3μm to 1 μm. For optical microstrutural examinations and carbon content measurements, the specimens were further etched with 4% Nital at room temperature for several seconds.

For SEM microstructural and EBSD crystallographic orientation examinations, the specimens were electronic polished in 8% perchloric acid ethanol solution at room temperature at the voltage of 30V for 10~15 seconds after mechanical polishing (paper polishing up to 2000#). It should be emphasized that the specimen preparation procedures of the non-field and field treated specimens (electrolytic polishing or etching, and rinsing) were strictly controlled to ensure identical preparation conditions, so that the output results from the non-field and the field treated specimens are comparable.

2.5.2 Optical microstructural examinations

The optical microstructure observations were performed with an OLYMPUS/BX61 microscope (The observation surface and the sample reference frame are shown in Figure 2.5). Phase fraction of the transformed microstructures and lamellar spacing of pearlite were analyzed with analySIS and averaged over certain number of analyzed areas. The details of the measurement information are displayed in Table 2.3.

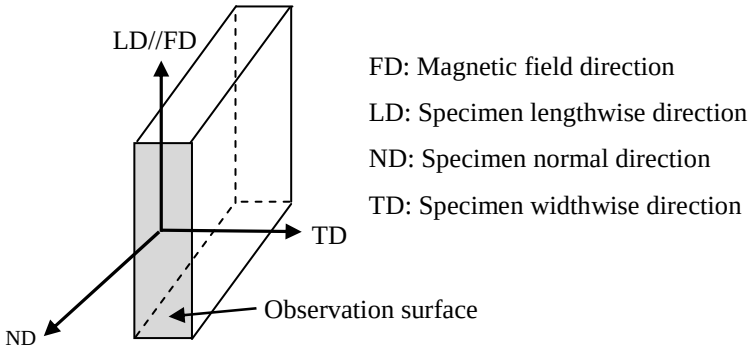

Figure 2.5 Schema of the observation area of the specimen.

Table 2.3 Information of microstructural measurements.

Fe-C alloys	Measurements	No. or area of measurements
Fe-0.12C	Area precentage of proeutectoid ferrite	15 areas
Fe-0.36C	Area precentage of proeutectoid ferrite	15 areas
	Area precentage of Widmanstätten ferrite	whole cross section(7mm×1mm)
Fe-1.1C	Area percentage of abnormal structure	whole cross section(10mm×3mm)
	Lamellar spacings of pearlite	20 areas

2.5.3 Wavelength-dispersive spectroscopic (EPMA) analysis

The carbon concentration of the proeutectoid ferrite in Fe-0.36C alloy was measured by means of wavelength-dispersive spectroscopy using a *Shimadzu 1610 electron probe microanalyzer* (WDS-EPMA). Six standard samples with carbon content ranging from 0.0075% to 0.978% were used to set the calibration curve for the WDS measurements. Both specimens treated without and with the magnetic field were examined during the same specimen loading to secure the identical measurement conditions for the non-field and field treated specimens. 20 proeutectoid ferrite areas in each specimen were randomly selected and measured to reach a global representation of the results.

2.5.4 Hardness tests

The hardness of proeutectoid ferrite in Fe-0.36C alloy was tested using a micro-indenter (diamond Vickers indenter Leitz, Wetzlar, Germany) with an applied load of 25g for 20s. The mean hardness was averaged over 8 measurements for each specimen.

2.5.5 Scanning electron microscopic and crystallographic orientation analysis

In this work, a field emission gun scanning electron microscope-*Jeol JSM 6500F* (the photo and the schematic illustration are displayed in Figure 6)-with EBSD acquisition camera and Oxford-HKL *Channel 5* software was used for microscopic and crystallographic orientation analyses. The working voltage was set at 15KV and the working distance was 15 mm.

For microscopic observations, the morphology of pearlitic cementite was examined and the area of spherical pearlite was measured in 20 randomly selected areas.

The crystallographic orientation analyses were performed for texture analyses and individual orientation measurements. The orientation data were obtained by acquiring and indexing the electron back-scatter diffraction Kikuchi patterns. The orientations are represented in the form of three *Euler angles (φ_1, Φ, φ_2)* in Bunge notation. The crystal structure data of ferrite and cementite for EBSD orientation measurements, are given in Table 2.4.

Table 2.4 Crystal structure data of ferrite and cementite.

Phase	Crystal structure/ Lattice parameters	Space group (No.)	Atomic position						
			No.	Atom	Wyckoff	X	Y	Z	Occupancy
Ferrite	*bcc* *a*=0.28665 nm.	*Im*$\bar{3}$*m (229)*	1	Fe	2a	0	0	0	1
Cementite	*orthorhombic* *a*=0.5090 nm *b*=0.6748 nm *c*=0.4523 nm	*Panm (62)*	1	C	4c	0.881	0.25	0.431	1
			2	Fe	4c	0.044	0.25	0.837	1
			3	Fe	8d	0.181	0.063	0.837	1

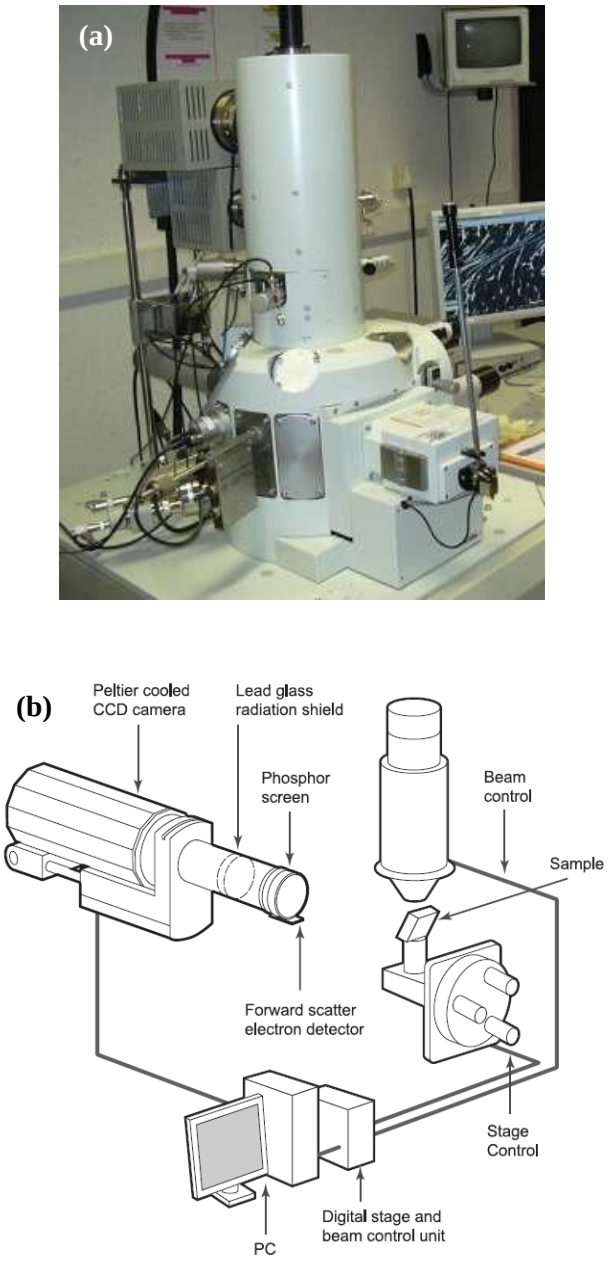

Figure 2.6 Photo (a) and schema (b) of the field emission gun SEM- *Jeol JSM 6500 F*.

In this work, two different beam controlled modes were applied for different orientation analysis purposes.

(1) Automated orientation mapping for massive orientation acquisition and for correlated microstructure and texture analyses.

The automated orientation mapping was performed to examine the orientation distribution of ferrite. As is known, ferrite is a simple-crystal-structured phase. The

orientation determination of ferrite by EBSD is usually efficient and accurate guaranteed by the attainable high-quality Kikuchi patterns form bulk ferrite grains and even from lamellar pearlitic ferrite. This ensures the orientation determination of ferrite from a large measurement area can be performed in the automatic mode within a short time. In this work, the automated mappings were performed on the whole cross section of the specimens at different step sizes, namely $0.5\mu m$, $1\mu m$, $2\mu m$ and $3\mu m$. As the crystal structure of cementite is relatively complicated and it is subject to a high level of internal constraint, within the same acquisition time for one Kikuchi pattern from ferrite, the acquired Kikuchi patterns of cementite is of very poor quality. Therefore, the measurement points on cementite always remain as non-indexed zero solution. The orientation information of pearlite colonies was only from their pearlitic ferrite. In this way, each pearlite colony is simply indentified as a ferrite grain. Finally, only the texture of ferrite (pearlitic and proeutectoid) was analyzed.

(2) Interactive mode for individual orientation measurements.

To investigate the orientation relationships (ORs) between ferrite and cementite in pearlite and in abnormal structure, individual orientations of ferrite and its neighboring cementite were measured. Due to the above-mentioned reasons for the nature of cementite together with the geometrical constrains imposed by the anisotropic shape of pearlitic cementite (thin lamellar: ~20nm in width) and the anisotropic shape of the electron beam when it touches the specimen surface under EBSD measurement chamber geometry (as shown in Figure 2.7), the correct and accurate orientation determination for cementite is difficult. The specimen has to be tilted at 70° from horizontal during the EBSD measurement, as a result, the electron beam was elongated along one (Y) direction, as illustrated in Figure 2.7. If the lamellar direction is perpendicular to this direction, the diffraction signal from

ferrite would be easily involved. To overcome these difficulties, special efforts have been made in ensuring the measurement reliability and accuracy. Several strategies are utilized in the present EBSD measurement work. (1) To get rid of the geometrical constrains imposed by the anisotropic shape of the thin pearlitic cementite and the elongated electron beam on the specimen surface that results in the acquisition of superposed Kikuchi patterns from both ferrite and cementite, the specimen is rotated around its surface normal axis to allow the lamellar length direction to be (as close as possible) parallel to the beam elongated direction for each analyzed pearlite colony. (2) To obtain high quality Kikuchi patterns of cementite, the number of acquisition cycle was increased to enhance the signal to noise ratio by increasing the number of "frame" at the Channel 5's Flamenco-EBSD acquisition layer. (3) To obtain high orientation determination accuracy, the maximum Hough resolution (125) at the Channel 5's Flamenco-EBSD acquisition layer was selected to ensure accurate band detections. One Kikuchi pattern acquired and indexed under the above measurement conditions as an example is shown in Figure 2.8. It is seen the raw pattern in Figure 2.8 (a) clearly displays the line details and recalculated pattern in (b) matches with the raw pattern, demonstrating that our strategies work well in ensuring the acquisition quality and the orientation determination quality.

To obtain a representative result of occurrence frequency of the appearing ORs, 15 colonies of pearlite were randomly selected for each specimen.

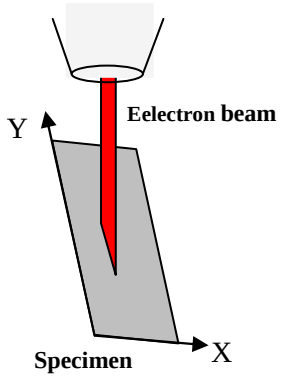

Figure 2.7 Geometry relation between the electron beam and the specimen surface under EBSD measurement condition. (The electron beam is elongated along the Y direction in the specimen coordinate system).

a

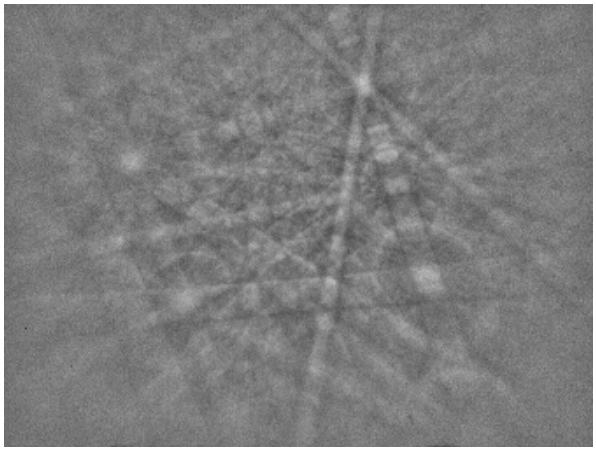

b

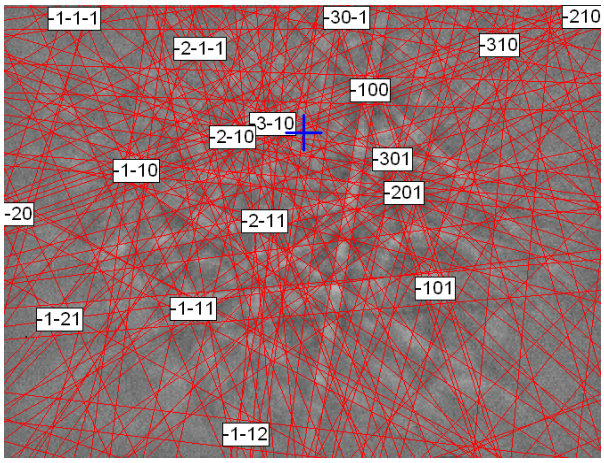

Figure 2.8 Kikuchi pattern of cementite (a) and the one superposed with the recalculated pattern (b).

2.5.6 Determination of orientation relationships between ferrite and cementite

In this work, the basic principle of the OR determination is to verify the direction-direction and plane-plane parallelisms between ferrite and cementite using the ORs between ferrite and cementite reported in literature. The utilized ORs are summarized in Table 2.5.

Table 2.5 Summary of the well-known and new ORs.

Well-known ORs	Expressed in Conventional way	New ORs [61]	Expressed in close-packed plane and in-plane direction
BAG	$[100]_C$ //$[1\bar{1}0]_F$ $[010]_C$ //$[111]_F$ Habit plane $(001)_C$ //$(11\bar{2})_F$	**Near BAG**	$(103)_C$ //$(01\bar{1})_F$ $[010]_C$ //$[111]_F$ Habit plane $(001)_C$ 3° *from* $(11\bar{2})_F$
IS	$(103)_C$ //$(01\bar{1})_F$ $[010]_C$ //$[111]_F$ Habit plane $(101)_C$ //$(11\bar{2})_F$	**P-P1**	$(103)_C$ //$(\bar{1}01)_F$ $[010]_C$ //$[131]_F$ Habit plane $(001)_C$ //$(\bar{2}\bar{1}5)_F$ $(103)_C$ //$(\bar{1}01)_F$ $(101)_C$ 8.7° *from* $(\bar{2}15)_F$
P-P	$[100]_C$ 2.6° *from* $[\bar{3}1\bar{1}]_F$ $[010]_C$ 2.6° *from* $[131]_F$ Habit plane $(001)_C$ //$(\bar{2}\bar{1}5)_F$	**P-P2**	$(103)_C$ //$(\bar{1}01)_F$ $[31\bar{1}]_C$ //$[111]_F$ Habit plane $(001)_C$ 3.5° *from* $(\bar{2}\bar{1}5)_F$ Unknown

The direction-direction and plane-plane parallelism verifications were performed by first transforming the corresponding direction vectors or plane normal vectors in the lattice basis of cementite (orthorhombic) to that of ferrite (cubic) by coordinate transformation using the determined orientation of ferrite and cementite by EBSD and then comparing them with the corresponding ferrite direction vectors or plane normal vectors to verify the parallelism between them to conclude the possible OR. The full OR determination process is detailed as follows.

(1) Setting of coordinate systems.

Three orthonormal coordinate systems have been chosen for convenience in addition to the crystal basis for ferrite and cementite. One is referred to the sample coordinate system. The second is to the crystal of ferrite that should be the same as the lattice basis of ferrite and the third one is to the crystal of cementite in a way that the corresponding basis vectors are parallel to lattice basis vectors (i.e.: $\vec{e_1} // \vec{a}$, $\vec{e_2} // \vec{b}$ and $\vec{e_3} // \vec{c}$). The difference between the two bases is that the crystal coordinate system of cementite is orthonormal, whereas the lattice basis is not.

(2) Construction of coordinate transformation matrices.

The coordinate transformation matrix G^j (*j=F* or *C*, where *F* denotes ferrite and *C* cementite) from the sample coordinate system to the ferrite/cementite coordinate system can be constructed using the *Euler angles* φ_1, Φ, φ_2 of ferrite/cementite with respect to the sample coordinate system determined by EBSD measurements.

$$G^j = \begin{pmatrix} \cos\varphi_1\cos\varphi_2 - \sin\varphi_1\sin\varphi_2\cos\Phi & -\cos\varphi_1\sin\varphi_2 - \sin\varphi_1\cos\varphi_2\cos\Phi & \sin\varphi_1\sin\Phi \\ \sin\varphi_1\cos\varphi_2 + \cos\varphi_1\sin\varphi_2\cos\Phi & -\sin\varphi_1\sin\varphi_2 + \cos\varphi_1\cos\varphi_2\cos\Phi & -\cos\varphi_1\sin\Phi \\ \sin\varphi_2\sin\Phi & \cos\varphi_2\sin\Phi & \cos\Phi \end{pmatrix} \tag{2.1}$$

Then, the coordinate transformation matrix from ferrite crystal coordinate system to cementite crystal coordinates system $\boldsymbol{\Delta G^{F\to C}}$ (as illustrated in Figure 2.9) can be calculated in matrix notation:

$$\left[G^F\right]\cdot\left[S^F\right]\cdot\left[\Delta G^{F\to C}\right] = \left[G^C\right]\cdot\left[S^C\right] \tag{2.2}$$

$$\left[\Delta G^{F\to C}\right] = \left[S^F\right]^{-1}\cdot\left[G^F\right]^{-1}\cdot\left[G^C\right]\cdot\left[S^C\right] \tag{2.3}$$

where S^F or S^C is the rotational symmetry matrix of crystal system of ferrite or cementite.

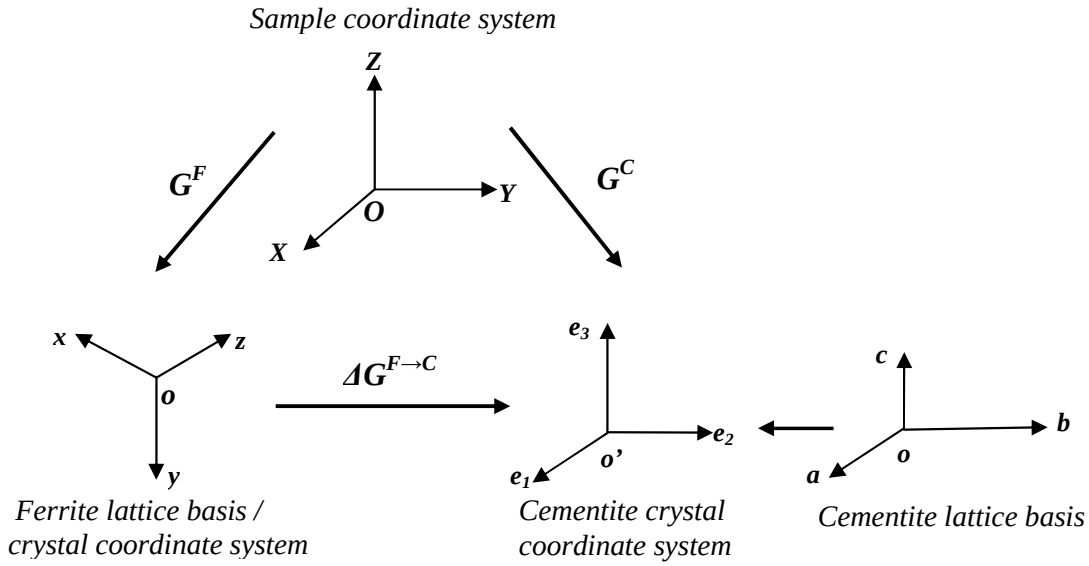

Figure 2.9 Coordinate system transformations from ferrite to cementite.

(3) Coordinate transformation of vectors

If one intends to transform the direction vectors or plane normal vectors in the cementite lattice basis to that of ferrite, the coordinate transformations start from cementite lattice basis between cementite crystal coordinate system, and followed by cementite crystal coordinate system between ferrite coordinates system (lattice basis).

For a direction vector [*u v w*] in cementite lattice basis, its corresponding direction vector in cementite coordinate system $\boldsymbol{v_C}$ is

$$v_C = ua\vec{e}_1 + vb\vec{e}_2 + wc\vec{e}_3 \tag{2.4}$$

where $\vec{e}_i$ (*i=1,2,3*) is the unit vector of cementite crystal coordinate system and *a, b, c* are the crystal lattice parameters of cementite. Then, the same vector in ferrite coordinate system v_F , can be calculated with the transformation matrices

$$v_F = \Delta G^{F \to C} v_C \tag{2.5}$$

For a normal vector of a plan (*h k l*) in cementite lattice basis, the coordinate transformation is more complicated. First, its normal vector in cementite lattice basis $\overrightarrow{g_{hkl}}$ can be represented by

$$\overrightarrow{g_{hkl}} = h\vec{a}^* + k\vec{b}^* + l\vec{c}^* \tag{2.6}$$

where $\vec{a}^*$, $\vec{b}^*$, $\vec{c}^*$ are the unit vectors of the cementite reciprocal lattice basis which can be calculated by the following equations:

$$\vec{a}^* = \frac{\vec{b} \wedge \vec{c}}{V},\ \vec{b}^* = \frac{\vec{c} \wedge \vec{a}}{V},\ \vec{c}^* = \frac{\vec{a} \wedge \vec{b}}{V} \tag{2.7}$$

where *V* is the volume of the unit cell built on the three cementite crystal lattice vectors $\vec{a},\ \vec{b},\ \vec{c}$.

$$V = \vec{a} \cdot (\vec{b} \wedge \vec{c}) = \vec{b} \cdot (\vec{c} \wedge \vec{a}) = \vec{c} \cdot (\vec{a} \wedge \vec{b}) \tag{2.8}$$

Thus,

$$\vec{a}^* = \frac{1}{a^2}\vec{a},\ \vec{b}^* = \frac{1}{b^2}\vec{b},\ \vec{c}^* = \frac{1}{c^2}\vec{c} \tag{2.9}$$

With equation (2.6) and (2.9), $\overrightarrow{g_{hkl}}$ can be obtained:

$$\overrightarrow{g_{hkl}} = \frac{h}{a^2}\vec{a} + \frac{k}{b^2}\vec{b} + \frac{l}{c^2}\vec{c} \tag{2.10}$$

Then, for the plane normal vector $\overrightarrow{g_{hkl}}$ [$\frac{h}{a^2}$ $\frac{k}{b^2}$ $\frac{l}{c^2}$] in cementite lattice basis, its corresponding vector in cementite coordinate system $\boldsymbol{v_C}$ can be obtained according to equation (2.4)

$$v_c = \frac{h}{a}\vec{e}_1 + \frac{k}{b}\vec{e}_2 + \frac{l}{c}\vec{e}_3 \tag{2.11}$$

And so the same vector in ferrite coordinate system can be calculated by equation (2.5).

(4) Angle between two vectors

As soon as the direction vectors or plane normal vectors of cementite are transformed into the same coordinates system with the corresponding vectors of ferrite, they can be compared.

We suppose $\vec{v}_1$ and $\vec{v}_2$ are two vectors in ferrite coordinates system. As it is known,

$$\vec{v}_1 \cdot \vec{v}_2 = \left|\vec{v}_1\right| \cdot \left|\vec{v}_2\right| \cdot \cos\left(\vec{v}_1 \hat{} \vec{v}_2\right) \tag{2.12}$$

Then,

$$\cos\left(\vec{v}_1 \hat{} \vec{v}_2\right) = \frac{\vec{v}_1 \cdot \vec{v}_2}{\left|\vec{v}_1\right| \cdot \left|\vec{v}_2\right|} \tag{2.13}$$

The angle $\boldsymbol{\Delta\delta}$ between two vectors can be calculated as following equation:

$$\Delta\delta = \arccos\left(\overrightarrow{v_1}\,\hat{}\,\overrightarrow{v_2}\right) = \arccos\left(\frac{\overrightarrow{v_1}\cdot\overrightarrow{v_2}}{\left|\overrightarrow{v_1}\right|\cdot\left|\overrightarrow{v_2}\right|}\right) \tag{2.14}$$

In the present work, if $\Delta\delta \leq 3°$ for the parallel directions and plane normals from ferrite and cementite, we consider that direction and plane parallelisms are fulfilled and the OR between ferrite and cementite is confirmed.

For the present study, the habit plane between ferrite and cementite in each OR was determined by the "indirect two-trace method" [62].

2.5.7 *Ab-initial* calculations

In order to interpret the working mechanism of the magnetic field on carbon solution in ferrite, the magnetic moments of *bcc* Fe and carbon atoms and the atomic magnetic dipolar interaction energy of Fe clusters without and with an interstitial carbon atom were evaluated. The calculations were carried out within the framework of density functional theory (DFT) using the Vienna *ab-initio* simulation package (VASP) [63, 64]. The interaction between ions and electrons was described by the projector augmented wave method (PAW) [65], and the exchange correlation potential was treated by the generalized gradient approximation (GGA) [66]. The pseudopotentials with $3d^7 4s^1$ and $2s^2 2p^2$ as respective valence states for Fe and carbon and a spin polarized representation of the electronic charge densities that allows for collinear description of magnetic moments were used. The kinetic energy cutoff was set to be 400eV and a Monkhorst-Pack [67] grid was employed to sample the Brillouin zone: 4×4×4 k-points sampling within a supercell containing 54 Fe atoms (27 *bcc* Bravais cells) and 1 carbon atom located in the octahedral interstice of the *bcc* Bravais cell at the center of the supercell (as illustrated in Figure 2.10). For comparison, the same calculations were performed on the same supercell but without the carbon atom.

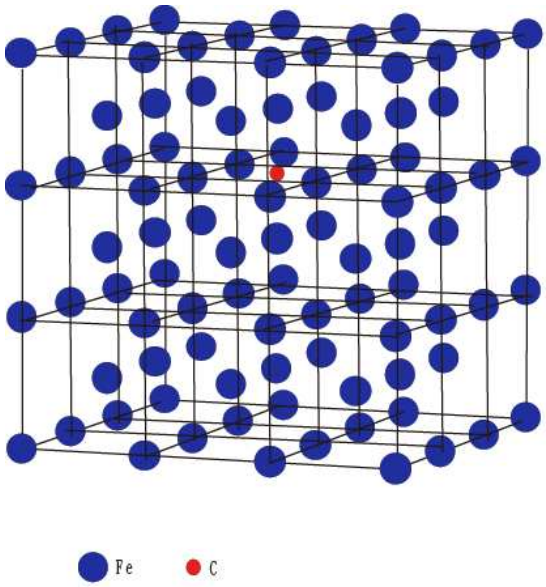

Figure 2.10 Supercell containing 54 Fe atoms and 1carbon atom.

Chapter 3

Magnetic-Field-Induced Microstructures Features during Austenitic Decomposition

Introduction

Magnetic field, like temperature and pressure, is one of the most important thermodynamic parameters which contribute to the Gibbs free energy of the materials. Therefore, magnetic field is capable of modifying the phase equilibrium and stability during diffusional phase transformations in steels. In this content, magnetic field shows its great potential in the domain of microstructural modification. As the mechanical properties and thus the performance of steels largely depend on its microstructure, better understandings of field influence and its influential mechanisms on microstructures are of critical significance. In this chapter, the magnetic-field-induced microstructures features during austenitic decomposition were thoroughly investigated in three Fe-C alloys by means of optical microscopy and SEM/EBSD.

In section 3.1, the magnetic-field-induced aligned and elongated microstructures were studied through a comparative examination of Fe-0.12C alloy and Fe-0.36C alloy. The magnetic field influential mechanism on the aligned and elongated microstructures was theoretically analyzed using the magnetic dipolar mode and discussed as a function of carbon content.

In section 3.2, the area fraction of the transformed ferrite was measured in both Fe-0.12C alloy and Fe-0.36C alloy. The effect of the magnetic field on modifying the amount of ferrite has been studied and discussed as a function of carbon content. Furthermore, the effect of the magnetic field on Widmänstatten ferrite has been studied in Fe-0.36C alloy.

In section 3.3, the effects of the magnetic field on the abnormal structure and the spheroidization of pearlite have been investigated in Fe-1.1C alloy. The morphology features as well as the crystallographic characteristics of the abnormal structure and the pearlite were studied.

3.1 Magnetic-field-induced aligned and elongated microstructures

Results

Figure 3.1 shows the microstructures of the Fe-0.12C alloy treated without and with the 12T magnetic field. It is seen that the transformed microstructures are both composed of proeutectoid ferrite (white) and pearlite (dark). Without the field, most ferrite grains and pearlite colonies are equiaxed. Though some others have elongated shapes, their major axes are randomly oriented. With the application of the 12T magnetic field, the pearlite colonies are obviously elongated along the field direction and moreover, many proeutectoid ferrite grains are aligned in chains along the field direction. Some of the ferrite grains are also elongated but with two elongation orientations: one is along the field direction and the other is perpendicular to the field direction. It can be seen that most of the elongated pearlite colonies are located between the ferrite chains.

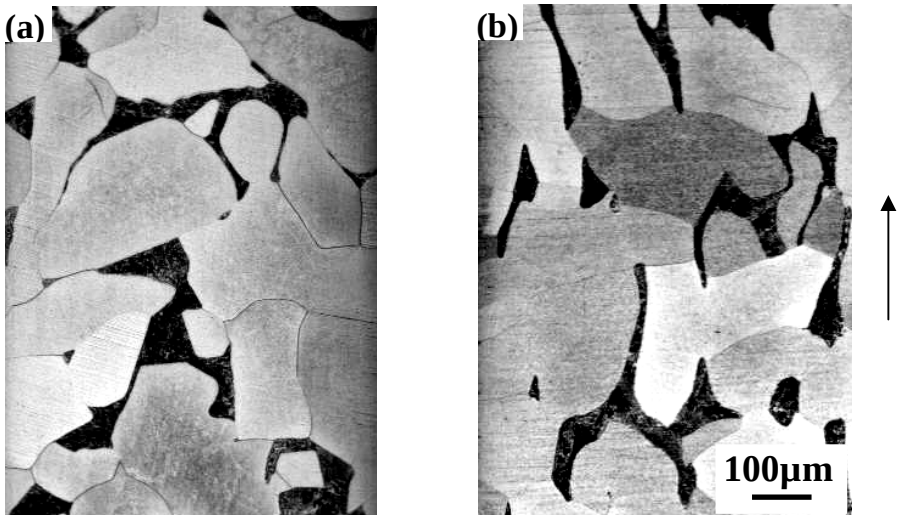

Figure 3.1 Microstructures of Fe-0.12C alloy without (a) and with (b) a 12T magnetic field. The arrow indicates the magnetic field direction.

For Fe-0.36C alloy, the transformed microstructures without and with the magnetic field are also composed of proeutectoid ferrite and pearlite, as shown in Figure 3.2. There are two kinds of proeutectoid ferrite with different morphologies: one is equiaxed, the other is acicular, known as Widmänstatten ferrite. Without the field, most of the proeutectoid ferrite is of Widmänstatten type, stretching through the thickness of the specimen. The proeutectoid ferrite and the pearlite colonies are basically randomly distributed, whereas with the field, the proeutectoid ferrite grains are obviously elongated along the field direction.

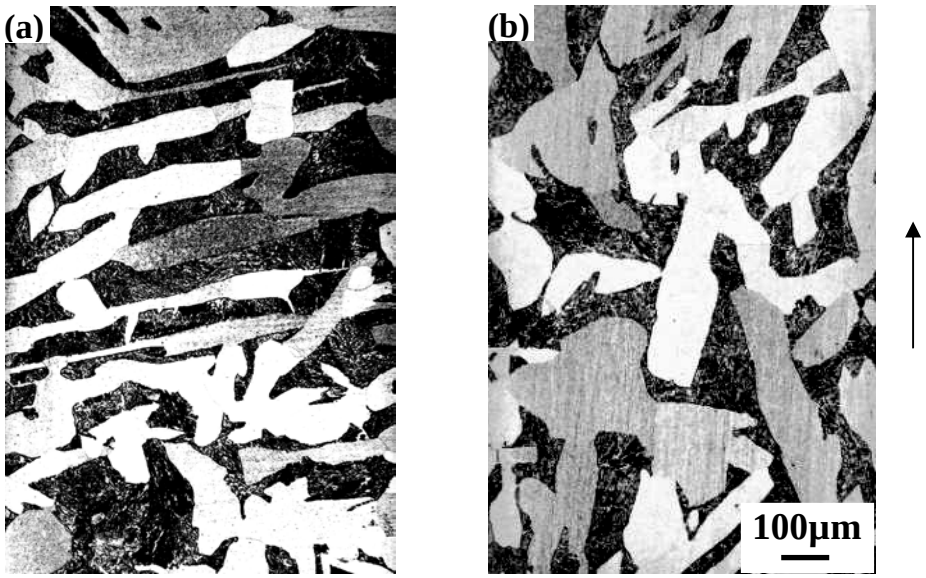

Figure 3.2 Microstructures of Fe-0.36C alloy without (a) and with (b) a 12T magnetic field. The arrow indicates the magnetic field direction.

It is seen that the transformed morphology features induced by the magnetic field in the Fe-0.12C alloy are quite different from those in the Fe-0.36C alloy. For the low carbon content Fe-0.12C alloy, the pearlite colonies are elongated along the field direction, while for Fe-0.36C alloy, the proeutectoid ferrite grains are obviously elongated along the field direction. This indicates the effect of the magnetic field on the aligned and elongated microstructure is carbon-content dependent.

Discussion

The field induced elongated and aligned microstructure during the proeutectoid ferritic transformation has been focused and studied in some iron-based alloys [34, 36, 50-53, 56, 58, 59]. It can be qualitatively explained by the magnetic dipole model [53, 60].

It is known that, under the magnetic field, the magnetic moments tend to align along the field direction, as schematically illustrated in Figure 3.3.

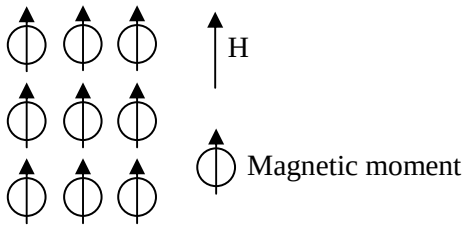

Figure 3.3 Schematic of the magnetic moments under the magnetic field.

Thus, there exists a dipolar interaction between the neighboring moments. The dipolar interaction energy E_D can be expressed as follows:

$$E_D = -\frac{\mu_0}{4\pi r_{12}^3}[3(\vec{m}_1 \cdot \vec{e}_{12})(\vec{m}_2 \cdot \vec{e}_{12}) - \vec{m}_1 \cdot \vec{m}_2] \tag{3.1}$$

where μ_0 is the vacuum magnetic permeability; $\vec{e}_{12}$ is a unit vector parallel to the line joining the centers of the two dipoles; r_{12} is the distance between two dipoles $\vec{m}_1$ and $\vec{m}_2$.

If the magnetic moments align along the field direction and $m_1 = m_2 = m$, $r_{12} = r$, the dipolar interaction energy E_D can be considered in the following two situations:

(1) The two magnetic dipoles are aligned in the magnetic field direction, as shown in Figure 3.4(a). Then the dipolar interaction energy between these two magnetic dipoles can be calculated as:

$$E_D = -\frac{\mu_0 m^2}{2\pi r^3} \tag{3.2}$$

since E_D is negative (E_D<0), the magnetic dipolar interaction between them is attractive, as a results, the magnetic dipoles tend to attract each other along the field direction.

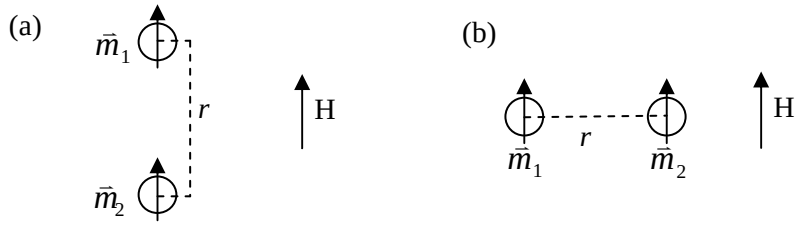

Figure 3.4 Illustration of the dipolar interaction between magnetic dipoles.
(a) The two magnetic dipoles are aligned along the magnetic field direction.
(b) The two magnetic dipoles are aligned in the transverse magnetic field direction.

(2) The two magnetic dipoles are aligned in the transverse magnetic field direction, as shown in Figure 3.4(b). Then the dipolar interaction energy between these two magnetic dipoles is resulted in:

$$E_D = \frac{\mu_0 m^2}{4\pi r^3} \tag{3.3}$$

It is seen that E_D is positive (E_D>0), which implies the magnetic dipolar interaction between them would make them repel each other in this direction.

As a result, under the magnetic field, magnetic dipoles attract each other along the field direction but repel each other along the transverse field direction due to the dipolar interaction.

During the austenite to ferrite and pearlite transformation, the magnetic dipolar interaction works in two scales: atomic-scale and micro-scale. In the atomic-scale, each Fe atom in ferrite grains carrying a magnetic moment can be regarded as a magnetic dipole. The magnetic dipolar interaction between them makes them attract each other along the field direction and repel each other in the transverse field direction. To minimize the demagnetization energy (caused by the repulsion) Fe atoms tend to align along the field direction. In this case, the effect of the magnetic field is mainly on grain growth process, which favors the elongation of the ferrite grains along the field direction. However, the elongation leads to an increase of the interfacial area and hence an increase of the interfacial energy which opposes the elongation and favors a spherical shape. The counterbalance between these two effects determines the final elongation degree of the grains [53, 58]. In the micro-scale, each magnetized ferrite grain can be regarded as a magnetic dipole. Due to the same magnetic dipolar interaction, new ferrite nuclei tend to nucleate next to the existing ones along the field direction and form ferrite chains to reduce the demagnetization energy. In this way, the nucleation of the ferrite is affected and the alignment is induced. As the alignment of both Fe atoms and the ferrite nuclei can reduce the demagnetization energy, they are energetically favored by the magnetic field. This is the reason for the formation of the elongated and aligned microstructure under the magnetic field.

In the present work, the carbon content of the Fe-0.12C alloy is relatively low. In this case, proeutectoid ferrite forms at high temperature, which is far above the Curie temperature, T_C. One could imagine that at the early stage of proeutectoid ferritic transformation which is above the T_C, the magnetic dipolar interaction in

both atomic-scale and micro-scale is weak, as the induced magnetization of ferrite and austenite are very close. Hence, ferrite nuclei form randomly at the prior austenite boundaries and grow uniformly. When the temperature drops down to the T_C, ferrite becomes ferromagnetic. As a consequence, the magnetic dipolar interaction in the two scales becomes stronger. Thus, both nucleation and grain growth in the subsequent cooling process is greatly influenced by the magnetic field. The new ferrite nuclei tend to form preferentially next to the existing ferrite grains along the field direction to form ferrite chains. It should be mentioned that as the carbon content of the alloy is low, the relative amount of proeutectoid ferrite is high and ferrite should be distributed densely in the specimen. This ensures small spacing between the existing ferrite grains and the new ferrite nuclei and hence strong micro-scale magnetic dipolar interaction between ferrite grains. Meanwhile, the existing ferrite grains preferentially grow along the field direction under the atomic dipolar interaction to form elongated grains. Since ferrite is in large quantity, its growth along the field direction may hinder the growth of the newly formed ferrite along that direction. Therefore, the growth of the new ferrite nuclei is restricted and occurs along the transverse field direction. As a result, the ferrite grains in two different elongation orientations are formed: the ferrite grains transformed at the early stage are elongated along the field direction, whereas those transformed at the late stage are elongated in transverse field direction. As ferrite is carbon depleted, the preferential nucleation and growth of proeutectoid ferrite along the field direction can cause the diffusion of carbon atoms in the field transverse direction. Hence, the remaining austenite between ferrite chains, especially next to the field-direction-elongated ferrite grains, is rich in carbon and provides perfect sites for the formation of pearlite. When temperature drops below Ar_1, this carbon-rich austenite located between ferrite chains decomposes into pearlite. As the

growth of the pearlite is restricted between the ferrite chains, the elongated pearlite colonies along the field direction are finally obtained.

As for the Fe-0.36C alloy, the proeutectoid ferrite transformation temperature is much lower than that of the Fe-0.12C alloy due to the increased carbon content. Though the ferrite transformation temperature is still above the T_C, the difference between them is reduced. Thus, the two-scaled magnetic dipolar interaction functions and affects the nucleation and growth of the proeutectoid ferrite, as most proeutectoid ferrite is transformed around and below T_C. However, as the carbon content is high, the relative amount of proeutectoid ferrite is low. The interspacing between ferrite grains is large. As the magnetic dipolar interaction energy E_D is proportional to r^{-3} (seen from Eq. 3.1), thus the micro-scaled dipolar interaction is reduced. As a result, transformed ferrite is mainly elongated in the field direction. No obvious field direction alignment is obtained compared with the case of Fe-0.12C alloy.

Summary

Magnetic field induces the elongated and aligned microstructures due to the effect of the magnetic dipolar interaction. During the austenitic decomposition process, the magnetic dipolar interaction works in two scales: atomic-scale and micro-scale. In atomic-scale, the grain growth process is influenced and the elongation of the nucleated grains in the field direction is resulted. In the micro-scale, the nucleation of the ferrite along the field direction is favored and the alignment is induced.

For the low carbon content Fe-0.12C alloy, the elongated pearlite colonies along the field direction are induced by the chained elongated ferrite grains in the field direction due to the effects of the atomic- and micro-scaled magnetic dipolar interaction on the nucleation and the growth of the ferrite around and below the T_C.

For the Fe-0.36C alloy, magnetic field elongates the proeutectoid ferrite grains in the field direction through atomic-scaled dipolar interaction during grain growth process.

This demonstrates magnetic field effect on inducing the elongated and aligned microstructures is carbon-content dependent.

3.2 Magnetic-field-induced phase fraction modification of ferrite

Results

The measurement results of ferrite area fraction of Fe-0.12C alloy and Fe-0.36C alloy treated without and with the magnetic field are shown in Figure 3.5. It shows that the magnetic field increases the amount of ferrite in both alloys. The field-induced increment in area fraction of ferrite is 6.0% in Fe-0.12C alloy and 14.0% in Fe-0.36C alloy. In this content, magnetic field enhances the formation of ferrite by increasing its area fraction and this field effect becomes more pronounced with the increase of the carbon content.

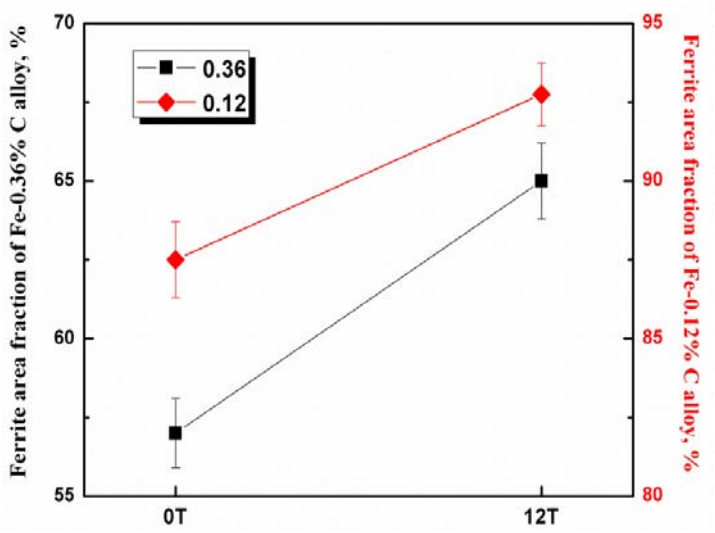

Figure 3.5 Ferrite area fraction of Fe-0.12C alloy and Fe-0.36C alloy treated without and with the 12T magnetic field.

The area fraction of Widmänstatten ferrite in Fe-0.36C alloy is measured and the result is given in Table 3.1. It is found that the amount of the Widmänstatten ferrite is greatly decreased with the application of the magnetic field.

Table 3.1 Area fraction of Widmänstatten ferrite in Fe-0.36C alloy treated without and with magnetic field.

Magnetic field	Area fraction of Widmänstatten ferrite, %
0T	48.44
12T	24.36

Discussion

When magnetic field is applied to proeutectoid ferritic phase transformation, both parent austenite and product ferrite can be magnetized and thus their Gibbs free energy is lowered according to their magnetization. The decrease in Gibbs free energy is expressed as

$$\Delta G = -\int_0^M \vec{B}_0 \cdot d\vec{M} \tag{3.4}$$

where M is the magnetization of a certain phase and B_0 is the induction of the applied magnetic field. Due to the fact that the magnetization of the product ferrite is higher than that of the parent austenite within the whole transformation temperature range, decrease in the Gibbs free energy of ferrite is higher. Hence, the energy difference between the parent austenite and the product ferrite is increased by the magnetic field. As a consequence, an extra energy term is introduced by magnetic field as a driving force to the austenite to ferrite phase transformation. Therefore, the phase transformation is accelerated by the magnetic field.

Previous simulation studies [28-33, 43, 68] have shown that magnetic field modifies the Fe-C phase equilibrium by shifting the $\alpha/\alpha+\gamma$ and the $\gamma/\alpha+\gamma$ boundaries in the Fe-C phase diagram towards the high carbon content and high temperature side, as shown in Figure 3.6. Moreover, it is proved that the field-influence on the

γ/α+γ boundaries is more pronounced. According to the 'Metallurgical Level Law', the amount of ferrite at eutectoid transformation temperature is proportional to the difference between the carbon solubility in austenite and the carbon content of the steel and inversely proportional to the carbon solubility difference between austenite and ferrite at the same temperature, i.e. $\frac{P(P')-C}{P-F(P'-F')}$, as schematically illustrated in Figure 3.6. Therefore, the amount of ferrite was increased by the magnetic field due to its influence on phase equilibrium.

The effect of the magnetic field on modifying the phase transformation temperature has been also discussed as the function of carbon content in Fe-based alloys. It is has been revealed by Garcin *et al*. [42] that, with the increase of the carbon content of the alloys, the increment of the Ae_3 temperature rises. However, the increment of the Ae_1 temperature does not change with the carbon content. As a result, the field effect on enhancing the area fraction of ferrite becomes more pronounced when the carbon content increases, as proved by this work.

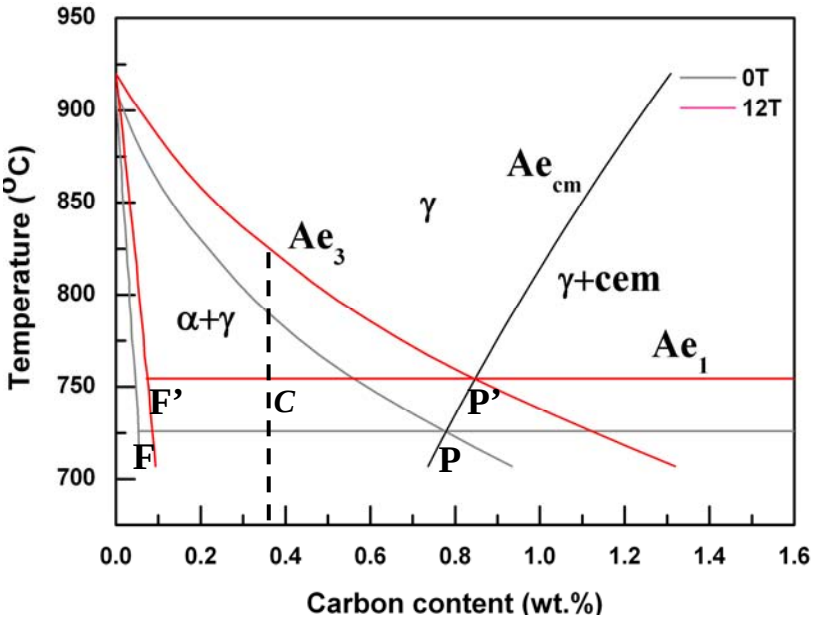

Figure 3.6 Effects of magnetic field on Fe-C phase equilibrium [49].

In addition, during the transformation from the parent austenite to ferrite, sometimes when the carbon content is suitable and the cooling rate is low, a kind of ferrite in acicular shape, known as Widmanstätten ferrite, of which the formation follows a K-S orientation relationship with the parent austenite, forms instead of the normal equiaxed ferrite. The formation of the Widmanstätten ferrite is considered to be resulted from the need to reduce the formation energy barrier when the dirving force is low [69].

According to the solid-state phase transformation theory, during the austenite to ferrite transformation, the Gibbs free energy changes related to uniform nucleation of a new phase can be express as

$$\Delta G = -V\Delta G_V + S\sigma + V\varepsilon \tag{3.5}$$

where V is the volume of the product phase, ΔG_V is the volume Gibbs free energy difference between the parent phase and the product phase. S is the surface area of the nuclei, σ is the interfacial energy between the parent phase and the product phase and ε is the elastic strain energy of the new phase. $V\Delta G_V$ is the driving force of the transformation, whereas, both $S\sigma$ -the total interfacial energy- and $V\varepsilon$ -the total elastic strain energy- are considered as the transformation barrier.

When austenite transforms into Widmanstätten ferrite, the K-S OR guarantees a low energy semi-coherent interface between the parent austenite and the product ferrite that greatly reduces the transformation barrier related to the interfacial energy. Considering of that, it is clear that the formation of Widmanstätten ferrite is due to the need of the reduction of the interfacial energy by forming coherent or semi-coherent interface, when the driving force is insuffient in the case of slow cooling.

As we mentioned before, when an external magnetic field is applied, an additional transformation driving force item is introduced by magnetic field.

$$\Delta G = -V(\Delta G_V + \Delta G_M) + S\sigma + V\varepsilon \tag{3.6}$$

Consequently, the need of forming low energy interface to compensate the insuffient driving force is reduced. Thus, the chance to form Widmanstätten ferrite is considerably lowered resulting in the reduced amount in the transformed microstructure of Fe-0.36C alloy under the magnetic field. As Widmanstätten ferrite is brittle and it is harmful to the ductility of steels, the field effect in reducing the amount of this ferrite is positive for its practical application.

Summary

Magnetic field increases the phase fraction of ferrite due to its thermodynamic influence on phase equilibrium. This field effect becomes more pronounced with the decreased austenite to ferrite transformation temperature that corresponds to the increased carbon content of steels.

Magnetic field reduces the formation of Widmanstätten ferrite by introducing an additional transformation driving force.

3.3 Magnetic field-induced microstructure features in Fe-1.1C alloy

Results

The microstructures of the Fe-1.1C alloy treated without and with the magnetic field and the corresponding pole figures of ferrite are displayed in Figure 3.7. As seen from the micrograph in Figure 3.7(a), without the magnetic field, the microstructure is composed of pearlite and a small amount of abnormal structure [70] (indicated by the arrow) that consists of coarse proeutectoid cementite distributed along the initial austenite grain boundaries and a border of ferrite surrounding it. From the pole figures in Figure 3.7 (a), it is seen that ferrite (ferrite in abnormal structure and pearlitic ferrite) does not display any preferred crystallographic orientation. When the 12T magnetic field is applied, as shown in Figure 3.7 (b), the microstructural constituents of the alloy remain the same (pearlite plus abnormal structure) and the crystallographic orientations of ferrite stays random, indicating that the magnetic field has no special effect on modifying the components of the microstructure and the crystallographic texture of ferrite. However, the magnetic field exhibits clear influence on the amount of the microstructural constituents, the morphology of the pearlite and the occurrence of the orientation relationships between ferrite and cementite in pearlite. Table 3.2 displays the total area percentage of the abnormal structure obtained without and with the 12T magnetic field. It is seen that the total area percentage of the abnormal structure is increased under the magnetic field, indicating that the magnetic field promotes the formation of the abnormal structure. Nevertheless, no specific OR between the cementite and the ferrite in the abnormal structure has been found either in the non-field- or in the field-treated specimen. This is different from what Chairuangsri *et al*. [71] reported. In their work, they found specific orientation

relationships (ORs) between the cementite and ferrite in the abnormal structure that are close to the Pitsch-Petch OR and the Bagaryatsky OR found in pearlite.

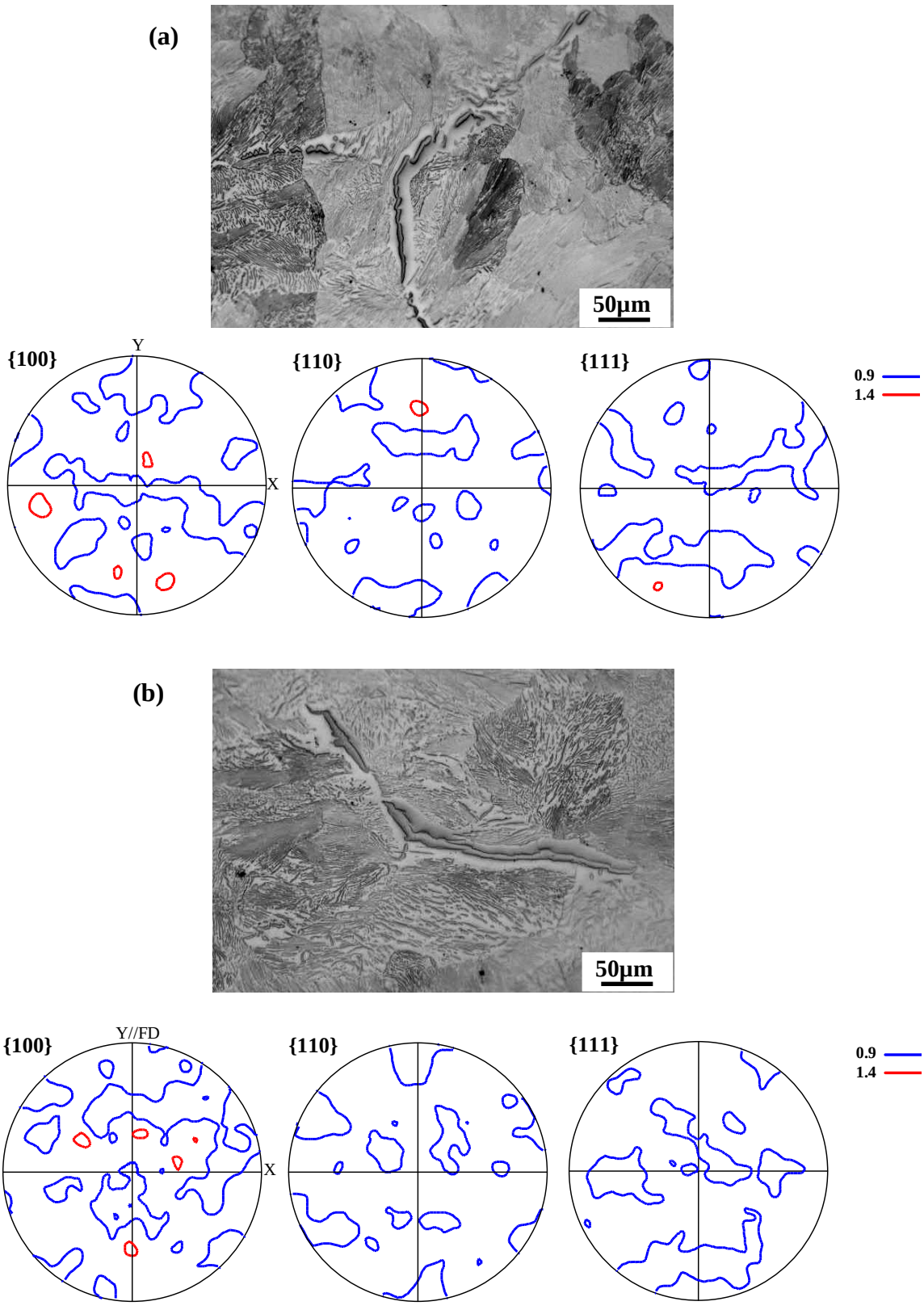

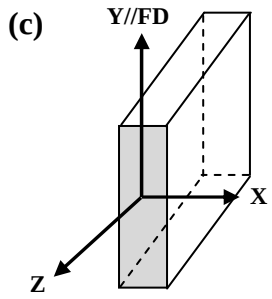

Figure 3.7 Optical micrographs and the corresponding pole figures of ferrite of Fe-1.1C alloy treated (a) without, (b) with a 12T magnetic field (the abnormal structure is indicated by the arrow; the field direction is horizontal) and (c) the corresponding sample coordinate system.

Table 3.2 Total area percentage of abnormal structure in Fe-1.1C alloy treated without and with a 12T magnetic field

Magnetic field	Total area percentage of abnormal structure, %
0T	0.18
12T	0.69

Figure 3.8 shows some typical pearlite colonies obtained without and with the magnetic field. It is seen that without the field, most of the pearlitic cementite are in lamellar shape (Figure 3.8(a)), whereas when the magnetic field is applied, the cementite tends to fragment and become short platelets or even spheroidal particles (Figure 3.8 (b)). It is known that pearlite colony with spheroidal cementite is called spheroidal pearlite. The area percentage of the spheroidal pearlite in the non-field- and the field-treated specimens are given in Table 3.3. It is seen that the amount of spheroidal pearlite is increased under the magnetic field. This indicates that the magnetic field promotes the spheroidization of cementite in pearlite. In addition, the average pearlite lamellar spacing is found enlarged from 0.47μm in the non-field-treated specimen to 0.9 μm in the field-treated specimen. This phenomenon has been observed in other steels and has been thoroughly analyzed [72, 73]. It is clear

that the area percentage of the abnormal structure and the morphology of the pearlitic cementite strongly depend on the orientation of the abnormal structures and the lamellar pearlite with respect to the observation plane (i.e. at which angle they intersect the observation plane). As there are no preferential crystallographic orientations in either the non-field- or the field-treated specimen, and the abnormal structures and the pearlite colonies are randomly selected with a substantial amount, the corresponding results on the abnormal structure and the pearlite could be considered only from the magnetic field.

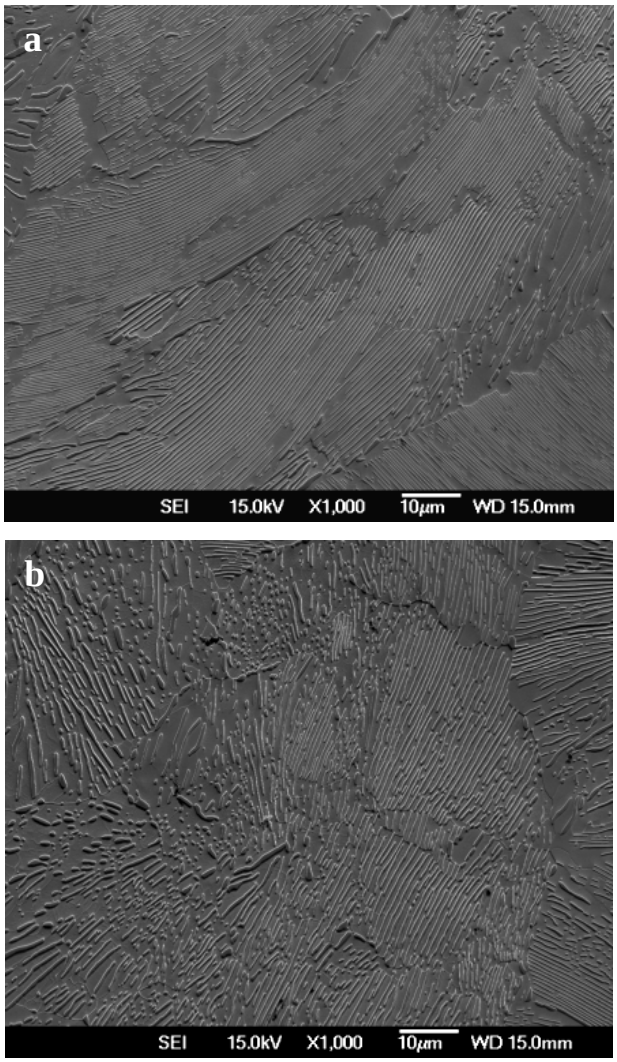

Figure 3.8 SEM secondary electron micrographs of transformed microstructure in Fe-1.1C alloys treated (a) without and (b) with a 12T magnetic field, the field direction is horizontal.

Table 3.3 Area percentage of the spherical pearlite in Fe-1.1C alloy treated without and with a 12T magnetic field.

Magnetic field	Area percentage of the spherical pearlite, %
0T	12.4
12T	27.1

Discussion

For a fully austenitized hypereutectoid steel, proeutectoid cementite first precipitates along the original austenite grain boundaries when the temperature drops to the range between Ar_{cm} and Ar_1 and then pearlite composed of lamellar cementite and ferrite forms from the remaining austenite when the temperature drops below Ar_1, during a slow cooling.

The formation of the ferrite border around the proeutectoid cementite that constitutes the so-called abnormal structure is due to the fact that the formation of the proeutectoid cementite along the initial austenite grain boundaries that is carbon enriched generates a carbon depleted zone in the vicinity of the proeutectoid cementite. If the depleted carbon cannot be resupplied from the interior of the austenite grain through carbon diffusion, the local composition will become hypoeutectoid, hence this part of austenite will transform into ferrite when the temperature is below Ar_3, forming the abnormal structure. The increase of the amount of abnormal structure by the magnetic field may be related to the influence of the magnetic field on phase equilibrium between austenite and ferrite. It is known that magnetic field promotes the formation of phases with higher induced magnetization during a transformation. In the case of the austenite to ferrite transformation, ferrite has higher magnetization than austenite; hence its formation is promoted by the magnetic field. In the present work, once the proeutectoid

cementite forms along the prior austenite boundaries, the carbon depleted austenite in its vicinity obtain a higher driving force under a magnetic field to transform to ferrite [30, 44, 45, 55]. As the magnetic field also shifts the eutectoid point to high carbon content side [29, 49] the amount of ferrite obtained is also increased, as widely observed in hypoeutectoid steels after its transformation from austenite to ferrite [30, 31, 42, 55]. Consequently, the amount of the abnormal ferrite surrounding the proeutectoid cementite is increased under the magnetic field.

For lamellar pearlite, spheroidization is a natural tendency, as in this process, the total interfacial area between ferrite and lamellar cementite can be reduced and then the total system becomes thermodynamically stable [74]. The influence of the magnetic field on spheroidization of pearlite may be related to two factors. First, spheroidization of pearlite is a carbon diffusion process [74-77]. As magnetic field elevates the proeutectoid transformation temperature [28, 42, 49, 72], pearlite forms at higher temperature under a magnetic field. High temperature favors carbon diffusion. Therefore, the spheroidization of pearlite that is realized by cementite fragmentation and granulation through carbon diffusion is enhanced by the magnetic field. Second, it has been revealed that magnetic field increases the relative interfacial energy between ferrite and cementite [45, 78], as the field has different impact on the magnetization of the boundary area and the grain interior. It is known that the Gibbs free energy of a crystal is lowered when it is magnetized. The degree of magnetization depends on the perfectness of the crystal in crystalline materials. As the boundary area possesses a high density of defects, the magnetization induced by a magnetic field is limited with respect to that of grain interior. The Gibbs free energy drop in grain interior is much higher than that in boundary area. As a result, the relative boundary energy is raised. Consequently, reducing the total boundary area thus the total boundary interfacial energy by spheroidization is energetically favored by the magnetic field.

Summary

Magnetic field promotes the formation of the abnormal structure through its influence on increasing the driving force of the carbon-depleted austenite to ferrite transformation. No specific OR between the cementite and the ferrite in the abnormal structure is found in the present study. Magnetic field enhances the spheroidization of pearlite through enhanced carbon diffusion resulting from the elevation of the transformation temperature and the increased relative ferrite/cementite interface energy from the magnetization difference between boundary areas and grain interiors.

Chapter 4

Magnetic Field-Enhanced Carbon Solution in Ferrite

Introduction

Strengthening has been widely required as one of the necessary properties for the deveplopment of high-performance structural materials. The most common strengthening mode refers to solid solution strengthening by adding various alloying elements, such as carbon in iron. As a promising technique for microstructure modification and texture control [36, 53, 58, 60, 79, 80], high magnetic field has shown its capacity to modify the solubility of phases in Fe-C alloy system, hence demonstrating great potential to enhance the effect of solid solution strenthening of steels.

According to thermodynamic calculations on phase equilibrium [28-32, 39, 68], the solubility of carbon in ferrite is increased under an applied magnetic field. Moreover, imposition of magnetic field increases the proeutectoid ferrite transformation temperature [29, 42, 45, 60] and enhances the phase fraction of the transformed ferrite [30, 31, 42, 55]. As ferrite is carbon-depleted and cementite is carbon-enriched in Fe-C system, a net increase in the amount of ferrite under a magnetic field requires a balanced carbon repartition bewteen the ferrite and cementite phases to maintain the fixed carbon content of the material. Hardness test of ferrite[7] has demonstrated that under a magnetic field ferrite becomes harder, indicating that the hardness increase is due to the increased carbon solution. Until now, however, there has been no direct experimental evidence for this assertion and the underlying physical mechanism of the field-induced carbon solubility remains to be addressed.

In the this chapter, the carbon concentrations of ferrite in the Fe-0.36C alloy treated without and with a 12T magnetic field were measured by means of wavelength-dispersive spectroscopy using a *Shimadzu 1610 electron probe microanalyzer* (WDS-EPMA). The hardness of proeutectoid ferrite was tested using a micro-indenter with a load of 25g. The mean hardness was calculated by averaging over 8 measurements for each specimen. In order to interpret the physical mechanism of the magnetic field on carbon solution in ferrite, the magnetic moments of *bcc* Fe and carbon atoms and the atomic magnetic dipolar interaction energy of Fe clusters without and with an interstitial carbon atom were evaluated. The calculations were carried out within the framework of density functional theory (DFT) using the Vienna *ab-initio* simulation package (VASP) [63, 64]. The interaction between ions and electrons was described by the projector augmented wave method (PAW) [65], and the exchange correlation potential was treated by the generalized gradient approximation (GGA) [66]. The pseudopotentials with $3d^7 4s^1$ and $2s^2 2p^2$ as respective valence states for Fe and carbon and a spin polarized representation of the electronic charge densities that allows for collinear description of magnetic moments were used. The kinetic energy cutoff was set to be 400eV and a Monkhorst-Pack [67] grid was employed to sample the Brillouin zone: 4×4×4 *k-points* sampling within a supercell containing 54 Fe atoms (27 *bcc* Bravais cells) and 1 carbon atom located in the octahedral interstice of the *bcc* Bravais cell at the center of the supercell. For comparison, the same calculations were performed on the same supercell but without the carbon atom.

Results

Figure 4.1 shows the microstructures of the specimens treated without and with the 12T magnetic field. The microstructures of both specimens are composed of proeutectoid ferrite (white) and pearlite (dark).

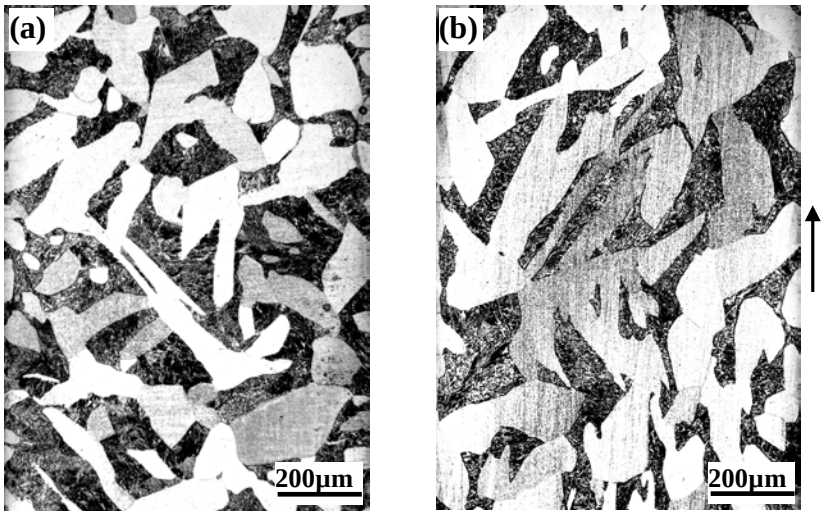

Figure 4.1 Microstructures of Fe-0.36C alloy treated without (a) and with (b) a 12T magnetic field. The arrow indicates the magnetic field direction.

The average area percentage and the average carbon content of proeutectoid ferrite of the non-field and field treated specimens are shown in Table 4.1 and Table 4.2, respectively. It is seen that the magnetic field increases the amount of proeutectoid ferrite by 14% and the carbon content in proeutectoid ferrite by 35.7%.

Table 4.1 Area percentages of proeutectoid ferrite in Fe-0.36C alloy treated without and with the 12T magnetic field (Number of measurements: 10).

Magnetic field	Area percentage of proeutectoid ferrite, (Standard deviation)	Increment
0T	57 (±1.1)%	--
12T	65 (±1.2)%	14%

Table 4.2 Carbon contents of proeutectoid ferrite in Fe-0.36C alloy treated without and with the 12T magnetic field (Number of measurements: 20).

Magnetic field	Carbon content of proeutectoid ferrite, (Standard deviation)	Increment
0T	0.14(±0.017)%	--
12T	0.19(±0.024) %	35.7%

For both specimens, the measurement carbon contents are higher than the theoretical values. This may come from two factors: the residual ethanol left from etching and rinsing during specimen preparation and the carbon contamination inside the EPMA column during the WDS measurements. Since the experimental conditions for the non-field and field treated specimens were strictly controlled to be identical, the carbon increments resulting from these two factors could be regarded as the same for the two specimens. Thus, the carbon content difference between the two specimens should be attributed to the magnetic field, as indirectly proved by the hardness tests (Table 4.3). Under the 12T magnetic field, the hardness of ferrite increases from $HV_{0.025}$ 88.1 to 102.1 by 15.9%, suggesting the solid solution strengthening of excessive carbon atoms in ferrite. In this regard, the field-induced increase in the amount of carbon-depleted ferrite is actually balanced by the elevation of their carbon content to maintain the fixed carbon content of the alloy.

Table 4.3 Mean hardness of proeutectoid ferrite in Fe-0.36C alloys treated without and with the 12T magnetic field (Number of measurements: 8).

Magnetic field	Mean hardness of proeutectoid ferrite, $HV_{0.025}$ (Standard deviation)	Increment
0T	88.1 (±2.71)	--
12T	102.1 (±6.86)	15.9%

Considering that the magnetic natures of Fe and carbon atoms are not the same, introducing a carbon atom into *bcc* Fe structure may modify the magnetic interaction between local atoms. The magnetic moments of Fe and carbon atoms calculated from *ab-initio* simulations are summarized in Table 4.4 and 4.5.

Table 4.4 Calculated magnetic moments carried by Fe atoms.
The *ab-initio* calculations were carried out using a supercell consisting of 54 Fe atoms.

Magnetic moments, (μ_B/atom)	Lattice constant, (Å)
2.151	2.81199

Table 4.5 Calculated magnetic moments carried by Fe and carbon atoms.
The *ab-initio* calculations were carried out using a supercell consisting of 54 Fe atoms with one carbon atom in the octahedral interstice of the centre *bcc* Bravais cell.

Magnetic moments, (μ_B/*atom*)			Lattice constant, (Å)
Fe	First neighbor	1.615	2.84018
	Second neighbor	2.178	
	Others	2.151	
Carbon		-0.119	

It is seen that without the carbon atom in the *bcc* Fe structure, the magnetic moments of Fe atoms are identical. When a carbon atom is introduced, the magnetic moments of Fe atoms vary with the neighborhood order to the carbon atom. The first (closest) neighbors of the Fe atoms to the carbon atom possess a smaller moment (1.615μ_B/atom) with respect to that (2.151 μ_B/*atom*) of the Fe atoms in the carbon free cell, whereas the second neighbors carry slightly larger moment (2.178 μ_B/atom). Starting from the third neighbors, the magnetic moments of Fe atoms resume to that in the carbon free cell. As a consequence of the modified magnetic moments, the magnetic interaction between these atoms is changed.

Discussion

It is known that when a magnetic field is applied, the moments of Fe atoms tend to align along the field direction. Each Fe or carbon atom can be regarded as a magnetic dipole and the interaction energy E_D between two magnetic dipoles can be calculated by Eq.(3.1) as discussed in Chapter 3. Then, the interaction energy E_D can be decomposed into two opposite contributions: the one giving rise to magnetization is negative, whereas the other resulting in demagnetization is positive. Clearly, the atomic structural configuration that enhances the magnetization contribution is preferred by the system.

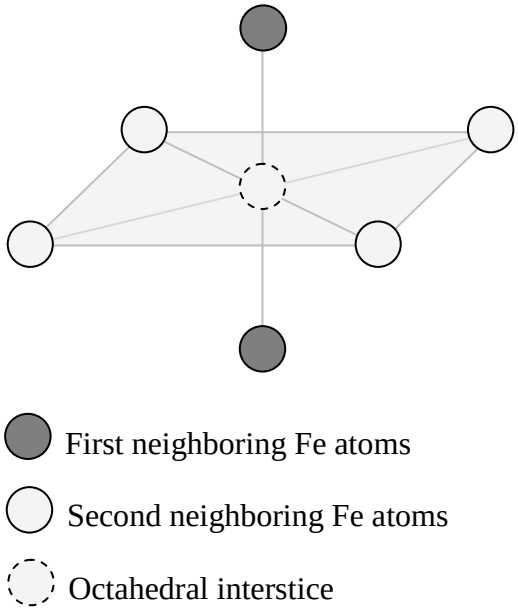

Figure 4.2 Octahedral interstice and its first and second neighboring Fe atoms in *bcc* structure.

Figure 4.2 illustrates an atom cluster that contains one octahedral interstice and its first and second neighboring Fe atoms in the *bcc* structure. When a carbon atom is present, it occupies the octahedral interstice. Suppose that the magnetic moments of the Fe atoms and the carbon atom are parallel to the field direction under the

magnetic field. The overall magnetic interaction energy over the atom cluster is then given by integrating the dipolar interaction of all atom pairs in the cluster, under the consideration that starting from the third neighbors, the Fe moments in the carbon containing cell are the same as those of their counterparts in the carbon free cell.

Accordingly, the magnetic interaction energies over the atom cluster without and with an interstitial carbon atom were calculated to be $3.0\times10^{-5}eV$ and $1.9\times10^{-5}eV$, respectively. The magnetic interactions in the two cases are both positive, indicating that the demagnetization contribution is more important than that of magnetization. However, when a carbon atom occupies the octahedral interstice, the interaction energy is decreased, *i.e.* the system becomes energetically more stable. This means that the magnetic field favors the solution of carbon atoms in the *bcc* Fe through reducing the demagnetization energy. In this way, the carbon content in ferrite is increased when a magnetic field is applied during the austenite to ferrite transformation.

Summary

The carbon content increase in ferrite induced by magnetic field has been experimentally demonstrated through the WDS-EPMA for the first time.

According to the *Ab-initio* calculations, the modified Fe magnetic moments originate from the carbon solution. When the magnetic moments of Fe atoms are aligned under an external magnetic field, the demagnetization energy due to atomic dipolar magnetic interaction is reduced with the carbon solution. This underlies the physical mechanism of field-enhanced carbon solution in ferrite.

Chapter 5

Magnetic-Field-Induced Crystallographic Orientation Characteristics

5.1 Magnetic-field-induced texture in hypo-eutectoid alloys

Introduction

As it is known, most mechanical properties of the materials are crystallographic anisotropic, so the performance of the materials usually depends on the microstructures as well as the crystallographic orientation. The preferential orientation distribution of polycrystallinematerials known as texture could be considerably strong in Fe-based alloys, which plays an important role in materials processing.

The field induced texture has been noticed and studied during magnetic annealing process in Fe based alloys. Martikainen *et al.* [81] reported the increase of the <001> texture component along the field direction and attributed this texture formation to the anisotropic magnetization in different crystallographic directions, as <100> direction is the easiest magnetization direction. Later, Zhang *et al.* [60] studied the effect of the magnetic field on texture of the ferrite during austenitic decomposition process and found the field-induced enhancement of <001> component along the transverse field direction in a medium carbon steel (0.49C). However, the similar texture component was not obtained in a 42CrMo steel [56]. This reveals the magnetic field influential mechanism on texture formation works differently and this field effect remains to be addressed.

In this chapter, the field-induced texture of ferrite was studied in two hypo-eutectoid alloys (Fe-0.12C alloy and Fe-0.36C alloy), the magnetic field influential

mechanism was analyzed as the function of magnetic field intensity and carbon content.

Results

The inverse pole figures of the proeutectoid ferrite in Fe-0.12C alloy treated without and with the 12T magnetic field are shown in Figure 5.1. The sample coordinate system is shown in Figure 5.2. It can be seen, there is no obvious preferential orientation of ferrite in the Fe-0.12C alloy.

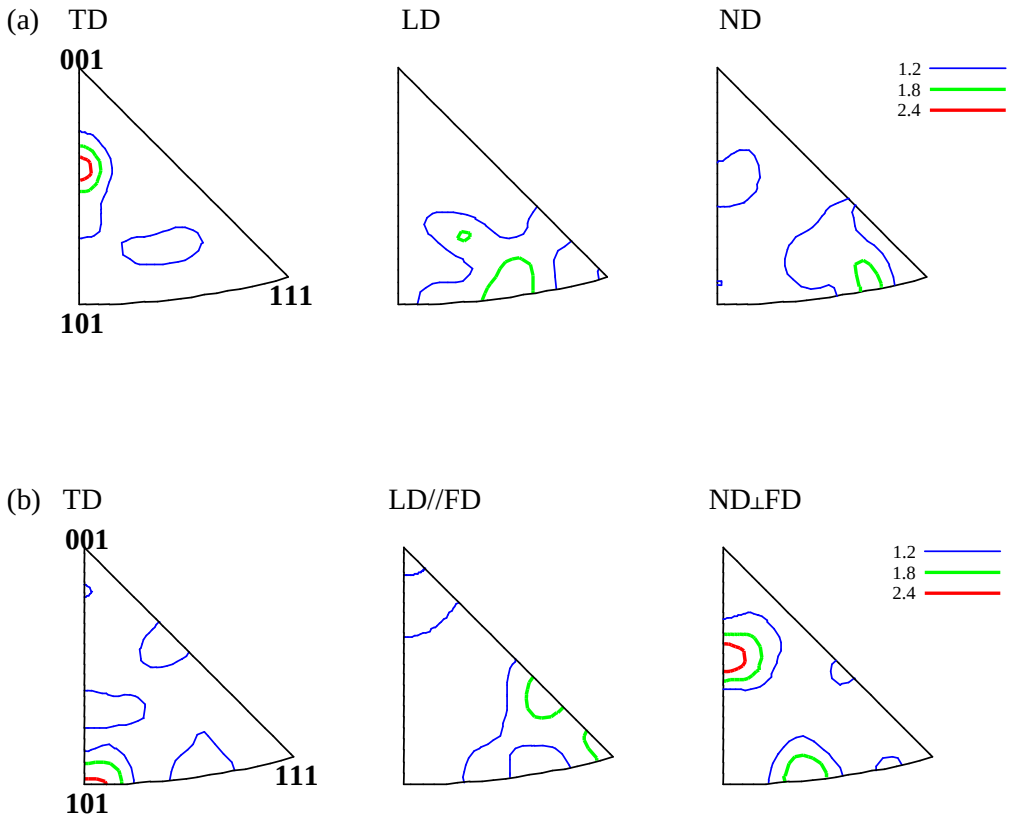

Figure 5.1 Inverse pole figures of ferrite in Fe-0.12C alloy treated without (a) and with (b) a 12T magnetic field.

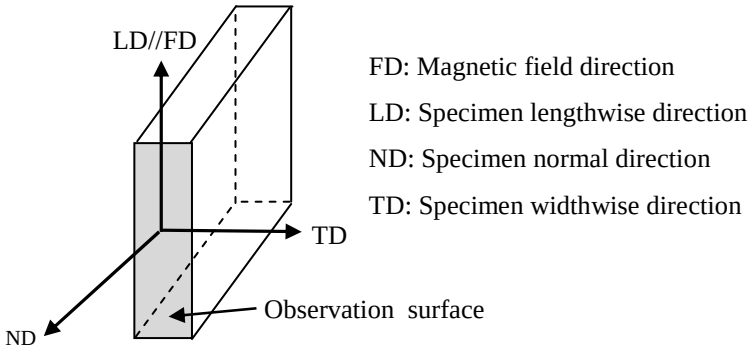

Figure 5.2 The sample coordinate system.

The inverse pole figures of ferrite in Fe-0.36C alloy treated without and with the application of the magnetic field are shown in Figure 5.3 (under the same sample coordinate system in Figure 5.2). In the Fe-0.36C alloy, an enhancement of <001> fiber component along the ND (transverse field direction) appears in the field treated specimens. Though this enhancement in 8T specimen is not obvious, it becomes much stronger when field is increased to 12 T.

Based on the above results, it is seen that the field induced ferrite texture is related to the field intensity and the carbon content of the alloys.

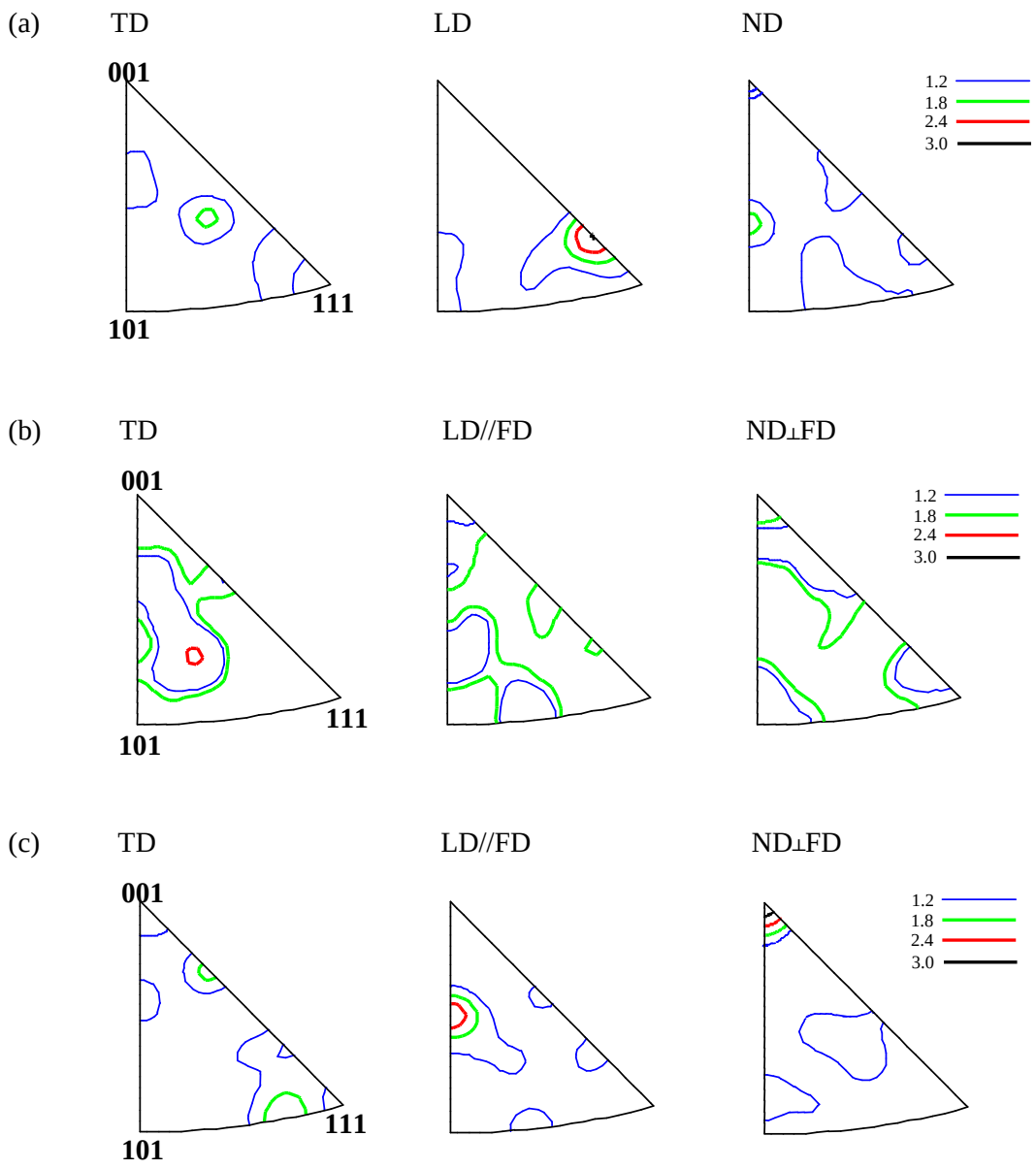

Figure 5.3 Inverse pole figures of the ferrite in Fe-0.36C alloy (a) 0T, (b) 8T and (C) 12T

Discussion

It is known that, when carbon atoms dissolve into ferrite, they occupy preferentially the octahedral interstices in the ferrite which are flattened in the <001> direction. As the atomic spacing between the two summate Fe atoms of the octahedral interstice in the <001> direction is smaller than the diameter of the

carbon atom, the carbon atom displaces the two Fe atoms in the opposite direction. This will generate the lattice distortion and thus distortion energy [60]. Since under the magnetic field, Fe atoms attract each other along the field direction and repels each other along the transverse field direction (the atomic dipolar interaction), the lattice distortion can be reduced by the increased atom spacing in the transverse field direction. If the distorted <001> direction is along the transverse field direction, the nucleation and growth of such ferrite grains will be energetically favored by the magnetic field. In this way, the <001> fiber component along the transverse field direction is enhanced. Obviously, this field effect is strongly related to the degree of lattice distortion of ferrite. Generally, the more the crystal lattice is distorted, the larger the distortion energy is. In this case, the need to reduce the distortion energy by favoring the growth of grain with their distorted <001> direction parallel to the transverse field direction would be increased. Consequently, the field effect appears stronger and the intensity of this <001> fiber component along the transverse field direction becomes enhanced. The degree of the lattice distortion is determined by two factors. One is the thermal expansion of the lattice which is temperature dependent and the other is the amount of oversaturated carbon atoms in ferrite when the transformation is non-equilibrium. For the Fe-0.36C alloy, the austenite to ferrite transformation happens at relatively lower temperature compared with that of the Fe-0.12C alloy. Carbon diffusion is restrained, and then more oversaturated carbon atoms will be left in the formed ferrite. Moreover, thermal expansion that the ferrite lattice can reach is also reduced. Thus, higher degree of lattice distortion could be expected in the Fe-0.36C alloy than in the Fe-0.12C alloy. As a result, the effect of the magnetic field on the texture of the proeutectoid ferrite is enhanced for the Fe-0.36C alloy, resulting in a visible enhancement of <001> fiber texture along the transverse field direction.

In addition, it is clear that the intensity of the <001> fiber component along the traverse field direction is directly related to the field intensity. For the present Fe-0.36C alloy, the visible enhancement of the <001> fiber texture requires high field intensity, i.e., 12T.

Summary

Due to the atomic-scaled magnetic dipolar interaction, magnetic field favors the nucleation and the growth of the ferrite grains with their distorted <001> direction parallel to the transverse field direction, and thus induces the enhancement of the <001> fiber component in the transverse field direction. This field effect is carbon content dependent. For low carbon content alloy (Fe-0.12C alloy), it is greatly reduced due to the reduced carbon oversaturation in ferrite and elevated formation temperature.

At the meantime, this field effect is also strongly related to the field intensity, as the enhancement of <001> fiber component along the transverse field direction becomes more pronounced with the increase of the magnetic field intensity. For Fe-0.36C alloy, a noticeable enhancement of <001> fiber component along the transverse field direction is detected under the 12T magnetic field.

5.2 Orientation relationships of pearlite under the magnetic field

Introduction

Pearlitic transformation, regarded as the most classic solid-solid state transformation, has been widely studied under the effect of magnetic field. The magnetic field influences on pearlitic transformation kinetics, mechanism of the pearlite formation and structure evolutions have been fruitful. It has been proved that magnetic field shows considerable effects on pearlitic transformation. It elevates the transformation temperature [39, 42, 49, 55], increases eutectoid carbon composition [49] and modifies the morphology of pearlite [72].

Nowadays, the investigations on the mechanism of the pearlitic transformation have been widely conducted from crystallographic point of view [61, 62, 82-102]. Several orientation relationships (ORs) between pearlitic ferrite and cementite have been consistently reported such as Isaichev OR [97], Bagaryatsky OR [102] and Pitsch-Petch OR [100, 101]. Recently, new ORs have been confirmed by Zhang *et.al* [61]. However, the effect of the magnetic field on the ORs of pearlite has been less studied yet.

Based on this, in this section, the ORs of pearlite in three high purity Fe-C alloys treated without and with the magnetic field have been examined by means of SEM/EBSD. The effect of the magnetic field on pearlitic ORs and their corresponding occurrence frequency are analyzed.

Results

The type of the ORs of pearlite found in this work has been summarized in Table 5.1. Three ferrite/cementite ORs were detected, namely, Isaichev OR denoted IS OR, and two near Pitsch-Petch ORs denoted P-P1 OR and P-P2 OR respectively

[61]. The types of the appearing ORs are the same in all the three alloys without and with the application of the magnetic field.

Table 5.1 Orientation relationships in pearlite.

IS OR	**P-P1 OR**	**P-P2 OR**
$(103)_C // (\bar{1}01)_F$	$(103)_C // (\bar{1}10)_F$	$(\bar{1}03)_C // (011)_F$
$[010]_C // [111]_F$	$[010]_C // [1\bar{1}3]_F$	$[311]_C // [1\bar{1}1]_F$
Habit plane	**Habit plane**	**Habit plane**
$(101)_C // (\bar{1}\bar{1}2)_F$	$(001)_C // (12\bar{5})_F$	$(001)_C 3.5° \mathit{from} (\bar{1}25)_F$

Although no change in the type of the appearing ORs is obtained, the corresponding occurrence frequency of each OR is evidently varied by the carbon content and the application of magnetic field, as illustrated in Table 5.2.

Table 5.2 Occurrence frequency of the appearing ORs in different Fe-C alloys.

Carbon content	Magnetic field	IS OR	P-P1 OR	P-P2 OR
Fe-0.12C	0T	43.8%	37.5%	18.8%
	12T	40.0%	40.0%	20.0%
Fe-0.36C	0T	46.7%	46.7%	6.7%
	12T	46.7%	40.0%	13.3%
Fe-1.1C	0T	33.3%	60.0%	6.7%
	12T	26.7%	53.3%	20.0%

It is noticed that, without the presence of the magnetic field, the IS OR is the most favorable OR in low carbon content steel (Fe-0.12C alloy), whereas, with the increase of the carbon content of the alloy, P-P1 OR tends to increase in the appearing number (Fe-0.36C alloy: 46.7% and Fe-1.1C alloy: 60.0%) at the expense

of mainly P-P2 OR. For all the alloys, the occurrence of P-P2 OR is much lower than the other two ORs.

When the magnetic field is applied, the occurrence frequency of the appearing ORs has been modified and it is found that the effect of the magnetic field is varied according to the carbon content of the alloys. For alloy with very low carbon (Fe-0.12C alloy), the effect of the magnetic field is rather limited indicating by a slight decrease in IS OR and small increase in both P-P1 and P-P2. When the carbon content increases, the effect of the magnetic field becomes pronounced. Magnetic field shows a consistent effect on increasing the number of P-P2 OR. This field effect is especially noticeable in Fe-1.1C alloy.

Discussion

It is known that when *fcc* austenite decomposes into dual-phase pearlite which consists of *bcc* ferrite and orthorhombic cementite, there exists two transformation barriers: one is the transformation strain energy caused by the lattice misfit at the austenite/ferrite [45] and austenite/cementite interfaces [83]; the other is the interfacial energy of the ferrite/cementite interface which depends on the atom misfit at the ferrite/cementite connecting plane [87]. To minimize the total transformation energy barrier, special ORs between the ferrite and the cementite in pearlite that ensure a low misfit interface between the parent and the product phase and a low misfit habit plane connecting the product phases are required. In terms of the three ORs obtained in the present work (IS, P-P1 and P-P2 OR), they all possess a common feature of closed-packed plane parallelism between the ferrite and the cementite, namely: $\{103\}_C//\{101\}_F$. Since the interplanar spacing of the $\{103\}_C$ and of the $\{101\}_F$ are both close to that of the closed-packed plane $\{111\}_A$ of austenite [61], the transformation strain at the austenite/ferrite and the austenite/cementite interface are minimized and hence leads to the minimum transformation strain

energy. In addition, it has been illustrated [61] that atoms from both the pearlitic ferrite and the pearlitic cementite are well matched at the connecting interface, which guarantees small interfacial energy under the three ORs in general. In view of the strain and the interfacial atomic mismatch, the IS and the P-P1 OR have the lowest formation energy barrier, so they are the more energetically favored and appear in large numbers. However, for the P-P2 OR, there is a 3.5° deviation in plane parallelism between the pearlitic ferrite and the pearlitic cementite at the connecting interface, therefore its occurrence is reduced, much less than the other two.

It has also been found that different ORs correspond to different nucleation situations. Previous work [61] has suggested that the IS OR could occur with either pearlitic ferrite or cementite nucleating first; the P-P1 OR happens when pearlitic ferrite and cementite nucleate simultaneously; while the P-P2 OR appears when pearlitic ferrite nucleates prior to pearlitic cementite. In this point of view, the frequency of P-P2 OR is expected to be low in high carbon alloys, as it is difficult to offer large low carbon content area in high carbon alloys for ferrite nucleation first. This is consistent with the results in this study.

In a hypereutectoid steel, with relatively high carbon content, austenite should possess high carbon content when austenite to pearlite transformation takes place. This composition characteristic is in favor of the formation of cementite or the simultaneous formation of cementite and ferrite. This is in good accordance with the present observation. As displayed in Table 5.2, the P-P1 and the IS OR account for the majority of the occurrence in the three ORs when the magnetic field is not applied. However, when the magnetic field is applied, the occurrence of the P-P2 OR is increased. As mentioned above, magnetic field promotes the formation of high magnetization phases [72]. In the pearlitic transformation temperature range, ferrite is ferromagnetic with higher magnetization and cementite is paramagnetic

with lower magnetization. The formation of ferrite is thus promoted by the magnetic field. Therefore, some low carbon concentration areas in austenite would transform to ferrite with the help of magnetic field before the formation of cementite. Consequently, the occurrence of the P-P2 OR, which corresponds to pearlitic ferrite nucleates first is increased by the magnetic field.

Summary

To minimum the transformation barriers, pearlitic ferrite and cementite follows specific ORs which guarantees the small transformation stains and the low atomic misfits, during the pearlite formation and growth process. Though magnetic field is able to offer additional driving force for this transformation and considerably raise the transformation temperature, it hardly overcomes the transformation strain energy barrier and the interfacial energy barrier to offer new ORs between the ferrite and the cementite in pearlite. As a result, the magnetic field has little influence on the type of the ORs appearing.

As magnetic field favors the nucleation of the high magnetization phase-pearlitic ferrite, the occurrence of the P-P2 OR that corresponds to the situation that pearlitic ferrite nucleates first, is increased by the magnetic field. This enhancement of the magnetic field on the occurrence of the P-P2 OR is more pronounced in high carbon content alloys, i.e. Fe-1.1C alloy.

Chapter 6 Conclusion and Perspectives

Conclusion

In this dissertation, the effect of the magnetic field on diffusional phase transformation has been thoroughly investigated in high purity Fe-C alloys theoretically and experimentally. Three high purity Fe-C alloys with different carbon content from both hypo- and hyper-eutectoid range were deliberately prepared. The effect of the magnetic field on microstructures features and crystallographic orientation characteristics of the transformed microstructures have been analyzed. The main achievements and conclusions have been drawn as follows.

6.1 Magnetic field induces new morphology features of microstructures.

(1) Due to the magnetic dipolar interaction, magnetic field induces the elongated and aligned microstructures in hypo-eutectoid alloys. This field effect is carbon-content dependent. The magnetic dipolar interaction works in two scales: atomic- and micro-scale. In the atomic scale, the magnetic dipolar interaction affects the grain growth process and results in the elongation; in the micro-scale, the magnetic dipolar interaction influences the nucleation process and introduces the alignment.

(2) Magnetic field promotes the formation of ferrite due to its thermodynamic influence on increasing eutectoid carbon composition. This field effect becomes more pronounced with the increase of the carbon content. Magnetic field inhibits the formation of Widmanstätten ferrite by introducing the additional driving force.

(3) Magnetic field promotes the formation of the abnormal structure by increasing the driving force of the transformation from carbon-depleted austenite to ferrite. There is no specific OR between ferrite and cementite in abnormal structure. Magnetic field enhances the spheroidization of pearlite through combination effect

of enhanced carbon diffusion resulting from the elevation of the transformation temperature and the increased relative ferrite/cementite interface energy from the magnetization difference between boundary areas and grain interiors.

6.2 Magnetic field enhances carbon solution in ferrite.

Carbon solution in ferrite affects the neighboring Fe magnetic moments, this leads to a decrease in the demagnetization energy which caused by the atomic dipolar magnetic interaction and makes the system more stable under the magnetic field. The field-induced carbon content enhancement offers a new possibility of material strengthening.

6.3 Magnetic field modifies the crystal orientation distribution of ferrite and affects the orientation relationship of pearlite.

(1) Magnetic field favors the nucleation and the growth of the ferrite grains with their distorted <001> direction parallel to the transverse field direction due to the atomic-scaled magnetic dipolar interaction, this leads to the enhancement of the <001> fiber component in the transverse field direction. This field effect is carbon content dependent. For low carbon content alloy (Fe-0.12C alloy), it is greatly reduced due to the reduced carbon oversaturation in ferrite and elevated formation temperature. For Fe-0.36C alloy, a noticeable enhancement of <001> fiber component along the transverse field direction is detected under the 12T magnetic field. At the meantime, this field effect is also strongly related to the field intensity, as the enhancement of <001> fiber component along the transverse field direction becomes more pronounced with the increase of the magnetic field intensity.

(2) Magnetic field can hardly change the type of the appearing ORs in pearlite. However, magnetic field promotes the nucleation of high magnetization phase-pearlitic ferrite and thus increases the occurrence of the P-P2 OR that corresponds to the situation that pearlitic ferrite nucleates first. This enhancement of the

magnetic field on the occurrence of the P-P2 OR is more pronounced in high carbon content alloys.

Perspectives

Up to date, the application of magnetic field has been popular in many areas of materials science. As the maturity of the magnetic field theory, plenty of magnetic field-induced phenomena have been discovered and well explained. However, better understanding of materials behavior under high magnetic field is still in need. Meanwhile, more physical phenomena are waiting to be revealed. Moreover, magnetic data, such as magnetic moment, *Tc* temperature, magnetic anisotropy, magnetostriction and so on, are waiting to be completed. New devices thus need to be developed for experimental measurements.

References

[1] M.A. Krivoglaz, V.D. Sadovskij, Effect of strong magentic fields on phase transformations, Physics of Metals and Metallography, 18 (1964) 23-27.

[2] V.D. Sadovskii, N.M. Rodigin, L.V. Smirnov, G.M. Filonchik, F.I. G, The question of the influence of magnetic field on martensitic transformation in steel, Physics of Metals and Metallography, 12 (1961) 131-133.

[3] Y.A. Fokina, L.V. Smirnov, V.D. Sadovskii, A.F. Peikul, Effect of a permanent magnetic field on the martensitic transformation in steel, Physics of Metals and Metallography, 19 (1965) 121-122.

[4] T. Kakeshita, K. Shimizu, T. Sakakibara, S. Funada, M. Date, Effects of a pulsed high magnetic field on the Ms temperature and martensite morphology in an Fe-31. 7at%Ni alloy, Scripta Metallurgica, 17 (1983) 897-900.

[5] T. Kakeshita, K. Shimizu, S. Funada, M. Date, Magnetic field-induced martensitic transformations in disordered and ordered Fe-Pt alloys, Transactions of the Japan Institute of Metals, 25 (1984) 837-844

[6] T. Kakeshita, K. Shimizu, S. Funada, M. Date, Composition dependence of magnetic field-induced martensitic transformations in Fe-Ni alloys, Acta Metallurgica, 33 (1985) 1381-1389.

[7] T. Kakeshita, K. Shimizu, T. Maki, I. Tamura, S. Kijima, M. Date, Magnetoelastic martensitic transformation in an ausaged Fe-Ni-Co-Ti alloy, Scripta Metallurgica, 19 (1985) 973-976.

[8] T. Kakeshita, K. Shimizu, S. Kijima, Z. Yu, M. Date, Magnetic field-induced martensitic transformations in Fe-Ni-C invar and non-invar alloys, Transactions of the Japan Institute of Metals, 26 (1985) 630-637

[9] T. Kakeshita, S. Furikado, K. Shimizu, S. Kijima, M. Date, Magnetic Field-Induced Martensitic Transformation in Single Crystals of Fe-31.6 at%Ni Alloy, Transactions of the Japan Institute of Metals, 27 (1986) 477-483

[10] T. Kakeshita, H. Shirai, K. Shimizu, K. Sugiyama, K. Hazumi, M. Date, Magnetic field-induced transformation from paramagnetic austenite to ferromagnetic martensite

in an Fe-3.9Mn-5.0C (at%) alloy, Transactions of the Japan Institute of Metals, 28 (1987) 891-897

[11] T. Kakeshita, H. Shirai, K. Shimizu, K. Sugiyama, K. Hazumi, M. Date, Effect of magnetic fields on martensitic transformations in alloys with a paramagnetic to antiferromagnetic transition in the austenitic state, Transactions of the Japan Institute of Metals, 29 (1988) 553-560

[12] T. Kakeshita, K. Shimizu, M. Ono, M. Date, Magnetic field-induced martensitic transformations in a few ferrous alloys, Journal of Magnetism and Magnetic Materials, 90–91 (1990) 34-36.

[13] T. Kakeshita, K. Kuroiwa, K. Shimizu, T. Ikeda, A. Yamagishi, M. Date, A new model explainable for both the athermal and isothermal natures of martensitic transformations in Fe-Ni-Mn alloys, Materials Transactions, JIM, 34 (1993) 423-428.

[14] T. Kakeshita, K. Kuroiwa, K. Shimizu, T. Ikeda, A. Yamagishi, M. Date, Effect of magnetic fields on athermal and isothermal martensitic transformations in Fe-Ni-Mn alloys, Materials Transactions, JIM, 34 (1993) 415-422.

[15] T. Kakeshita, T. Yamamoto, K.i. Shimizu, K. Sugiyama, S. Endo, Effects of static magnetic field and hydrostatic pressure on the isothermal martensitic transformation in a Fe-Ni-Mn alloy, Materials Transactions, JIM, 36 (1995) 1018-1022.

[16] T. Kakeshita, T. Fukuda, T. Saburi, K. Kindo, S. Endo, Effects of magnetic field and hydrostatic pressure on martensitic transformation process in some ferrous alloys, Physica B: Condensed Matter, 237–238 (1997) 603-604.

[17] T. Kakeshita, T. Saburi, K. Kindo, S. Endo, Effect of magnetic field and hydrostatic pressure on martensitic transformation and its kinetics, Japanese Journal of Applied Physics, 36 (1997) 7083-7094.

[18] T. Kakeshita, T. Saburi, K. Kind, S. Endo, Martensitic transformations in some ferrous and non-ferrous alloys under magnetic field and hydrostatic pressure, Phase Transitions, 70 (1999) 65-113.

[19] T. Kakeshita, T. Saburi, K. Shimizu, Effects of hydrostatic pressure and magnetic field on martensitic transformations, Materials Science and Engineering: A, 273–275 (1999) 21-39.

[20] T. Kakeshita, T. Takeuchi, T. Fukuda, T. Saburi, R. Oshima, S. Muto, K. Kishio, Magnetic field-induced martensitic transformation and giant Magnetostriction in Fe-Ni-Co-Ti and ordered Fe_3Pt shape memory alloys, Material Transactions, JIM, 41 (2000) 882-887.

[21] T. Kakeshita, J. Katsuyama, T. Fukuda, T. Saburi, Time-dependent nature of displacive transformations in Fe–Ni and Fe–Ni–Mn alloys under magnetic field and hydrostatic pressure, Materials Science and Engineering: A, 312 (2001) 219-226.

[22] S.A. Grishin, Structure and properties of structural steels after isothermal treatment in a magnetic field, Metal Science and Heat Treatment, 29 (1987) 882-886.

[23] H.K.D.H. Bhadeshia, Bainite in Steels, (2001).

[24] H. Ohtsuka, Effects of a high magnetic field on bainitic transformation in Fe-based alloys, Materials Science and Engineering: A, 438-440 (2006) 136-139.

[25] H. Ohtsuka, Effects of strong magnetic fields on bainitic transformation, Current Opinion in Solid State and Materials Science, 8 (2004) 279-284.

[26] V.D. Sadovskii, Magnetic field and phase transformations in steel, Metal Science and Heat Treatment, 7 (1965) 441-443.

[27] A.K. Ghosh, M.N. Roy, Phase tranformation of steel in magnetic field Transactions of Indian Institute of Metals, 40 (1987) 329-333.

[28] H.D. Joo, S.U. Kim, N.S. Shin, Y.M. Koo, An effect of high magnetic field on phase transformation in Fe–C system, Materials Letters, 43 (2000) 225-229.

[29] H. Joo, S. Kim, Y. Koo, N. Shin, J. Choi, An effect of a strong magnetic field on the phase transformation in plain carbon steels, Metallurgical and Materials Transactions A, 35 (2004) 1663-1668.

[30] J.K. Choi, H. Ohtsuka, Y. Xu, W.Y. Choo, Effects of a strong magnetic field on the phase stability of plain carbon steels, Scripta Materialia, 43 (2000) 221-226.

[31] M. Enomoto, H. Guo, Y. Tazuke, Y. Abe, M. Shimotomai, Influence of magnetic field on the kinetics of proeutectoid ferrite transformation in iron alloys, Metallurgical and Materials Transactions A, 32 (2001) 445-453.

[32] H. Guo, M. Enomoto, Influence of magnetic fields on γ-α equilibrium in Fe-C(-X) alloys, Materials Transactions, JIM, 41 (2000) 911-916.

[33] X. Hao, H. Ohtsuka, Effect of High Magnetic Field on Phase Transformation Temperature in Fe-C Alloys, Materials Transactions, JIM, 45 (2004) 2622-2625.

[34] X.J. Hao, H. Ohtsuka, P.D. Rango, H. Wada, Quantitative Characterization of the Structural Alignment in Fe-0.4C Alloy Transformed in High Magnetic Field, Anglais, 44 (2003) 211-213.

[35] X.J. Hao, H. Ohtsuka, H. Wada, Structural elongation and alignment in a Fe-0.4C alloy by isothermal ferrite transformation in high magnetic fields, Materials Transactions, JIM, 44 (2003) 2532-2536.

[36] H. Ohtsuka, Y. Xu, H. Wada, Alignment of ferrite grains during austenite to ferrite transformation in a high magnetic field, Materials Transactions, JIM, 41 (2000) 907-910.

[37] H. Ohtsuka, X.J. Hao, H. Wada, Effects of magnetic field and prior austenite grain size on the structure formed by reverse transformation from lath martensite to austenite in an Fe-0.4C alloy, Materials Transactions, JIM, 44 (2003) 2529-2531.

[38] H. Ohtsuka, Structural control of Fe-based alloys through diffusional solid/solid phase transformations in a high magnetic field, Science and Technology of Advanced Materials, 9 (2008) 013004.

[39] Y.D. Zhang, C.S. He, X. Zhao, Y.D. Wang, L. Zuo, C. Esling, Calculation of magnetization and phase equilibrium in Fe-C binary system under a magnetic field Solid State Phenomena 105 (2005) 187-194.

[40] T. Fukuda, M. Yuge, T. Terai, T. Kakeshita, Magnetic field dependence of γ-α equilibrium temperature in Fe-Co alloys, Journal of Physics: Conference Series, 51 (2006) 307-310.

[41] S. Farjami, M. Yuge, T. Fukuda, T. Terai, T. Kakeshita, Effect of Magnetic Field on γ-α Transformation in Fe-Rh Alloys, Anglais, 48 (2007) 2821-2825.

[42] T. Garcin, S. Rivoirard, C. Elgoyhen, E. Beaugnon, Experimental evidence and thermodynamics analysis of high magnetic field effects on the austenite to ferrite transformation temperature in Fe–C–Mn alloys, Acta Materialia, 58 (2010) 2026-2032.

[43] T. Garcin, S. Rivoirard, E. Beaugnon, Thermodynamic analysis using experimental magnetization data of the austenite/ferrite phase transformation in Fe–

xNi alloys (x= 0, 2, 4 wt%) in a strong magnetic field, Journal of Physics D: Applied Physics, 44 (2011) 015001.

[44] T. Garcin, S. Rivoirard, E. Beaugnon, In situ characterization of phase transformations in a magnetic field in Fe-Ni alloys, Journal of Physics: Conference Series, 156 (2009) 012010.

[45] T. Garcin, S. Rivoirard, F. Gaucherand, E. Beaugnon, Kinetic effects of magnetic field on the γ/α interface controlled reaction in iron, Journal of Applied Physics, 107 (2010) 103903.

[46] S. Rivoirard, T. Garcin, E. Beaugnon, F. Gaucherand, High temperature dilatation measurements by in situ laser interferometry under high magnetic field, Review of Scientific Instruments, 80 (2009) 103901.

[47] F. Gaucherand, E. Beaugnon, Magnetic susceptibility of high-Curie-temperature alloys near their melting point Physica B: Condensed Matter, 294 (2001) 96-101.

[48] Y.D. Zhang, C. Esling, M. Calcagnotto, M.L. Gong, H. Klein, X. Zhao, L. Zuo, Effect of a high magnetic field on eutectoid point shift and texture evolution in 0.81C-Fe steel, Texture, Stress, and Microstructure, 2008 (2008).

[49] Y.D. Zhang, C. Esling, M. Calcagnotto, M.L. Gong, X. Zhao, L. Zuo, Shift of the eutectoid point in the Fe-C binary system by a high magnetic field, Journal of Physics D: Applied Physics, 40 (2007) 6501-6506.

[50] M. Shimotomai, K.I. Maruta, Aligned of two-phase structures in Fe-C alloys, Scripta Materialia, 42 (1999) 499-503.

[51] K. Maruta, M. Shimotomai, Magnetic field-induced alignment of steel microstructures, Journal of Crystal Growth, 237-239, Part 3 (2002) 1802-1805.

[52] K. Maruta, M. Shimotomai, Alignment of two-phase structures in Fe-C alloys by application of magnetic field, Material Transactions, JIM, 41 (2000) 902-906.

[53] M. Shimotomai, K. Maruta, K. Mine, M. Matsui, Formation of aligned two-phase microstructures by applying a magnetic field during the austenite to ferrite transformation in steels, Acta Materialia, 51 (2003) 2921-2932.

[54] X. Hao, H. Ohtsuka, Effects of a High Magnetic Field on Transformation Temperatures in Fe-based Alloys, ISIJ International, 46 (2006) 1271-1273.

[55] Y.D. Zhang, C. He, X. Zhao, L. Zuo, C. Esling, Thermodynamic and kinetic characteristics of the austenite-to-ferrite transformation under high magnetic field in medium carbon steel, Journal of Magnetism and Magnetic Materials, 294 (2005) 267-272.

[56] Y. Zhang, C. He, X. Zhao, L. Zuo, C. Esling, J. He, New microstructural features occurring during transformation from austenite to ferrite under the kinetic influence of magnetic field in a medium carbon steel, Journal of Magnetism and Magnetic Materials, 284 (2004) 287-293.

[57] Y. Zhang, C. He, X. Zhao, C. Esling, L. Zuo, A new approach for rapid annealing of medium carbon steels, Advanced Engineering Materials, 6 (2004) 310-313.

[58] Y.D. Zhang, C. Esling, J. Muller, C.S. He, X. Zhao, L. Zuo, Magnetic-field-induced grain elongation in a medium carbon steel during its austenitic decomposition, Applied Physics Letters, 87 (2005) 212504.

[59] J.Y. Song, Y.D. Zhang, X. Zhao, L. Zuo, Effects of high magnetic field strength and direction on pearlite formation in Fe–0.12%C steel, Journal of Materials Science, 43 (2008) 6105-6108.

[60] Y.D. Zhang, C. Esling, J.S. Lecomte, C.S. He, X. Zhao, L. Zuo, Grain boundary characteristics and texture formation in a medium carbon steel during its austenitic decomposition in a high magnetic field, Acta Materialia, 53 (2005) 5213-5221.

[61] Y. Zhang, C. Esling, M. Calcagnotto, X. Zhao, L. Zuo, New insights into crystallographic correlations between ferrite and cementite in lamellar eutectoid structures obtained by SEM–FEG/EBSD and an indirect two-trace method, Journal of Applied Crystallography, 40 (2007) 849-856.

[62] Y.D. Zhang, C. Esling, X. Zhao, L. Zuo, Indirect two-trace method to determine a faceted low-energy interface between two crystallographically correlated crystals, Journal of Applied Crystallography, 40 (2007) 436-440.

[63] G. Kresse, J. Furthmüller, Efficient iterative schemes for ab initio total-energy calculations using a plane-wave basis set, Physical Review B, 54 (1996) 11169-11186.

[64] G. Kresse, D. Joubert, From ultrasoft pseudopotentials to the projector augmented-wave method, Physical Review B, 59 (1999) 1758-1775.

[65] P.E. Blöchl, Projector augmented-wave method, Physical Review B, 50 (1994) 17953-17979.

[66] J.P. Perdew, K. Burke, M. Ernzerhof, Generalized gradient approximation made simple, Physical Review Letters, 77 (1996) 3865-3868.

[67] H.J. Monkhorst, J.D. Pack, Special points for Brillouin-zone integrations, Physical Review B, 13 (1976) 5188-5192.

[68] M.C. Gao, T.A. Bennett, A.D. Rollett, D.E. Laughlin, The effects of applied magnetic fields on the α/γ phase boundary in the Fe–Si system, Journal of Physics D: Applied Physics, 39 (2006) 2890-2896.

[69] S. Wang, X. Zhao, Y.D. Zhang, L. Zuo, C. Esling, Effect of a high magnetic field on the formation of Widmänstatten ferrite in Fe-0.52C, Materials Transactions, JIM, 48 (2007) 2816-2820.

[70] H.W. McQuaid, E.W. Ehn, Effect of quality of steel on case-carburizing results, Trans. Am. Inst. Min. Engrs,, 67 (1922) 341-391.

[71] T. Chairuangsri, D.V. Edmonds, Abnormal ferrite in hyper-eutectoid steels, Acta Materialia, 48 (2000) 1581-1591.

[72] Y.D. Zhang, C. Esling, M.L. Gong, G. Vincent, X. Zhao, L. Zuo, Microstructural features induced by a high magnetic field in a hypereutectoid steel during austenitic decomposition, Scripta Materialia, 54 (2006) 1897-1900.

[73] Y. Zhang, G. Vincent, N. Dewobroto, L. Germain, X. Zhao, L. Zuo, C. Esling, The effects of thermal processing in a magnetic field on grain boundary characters of ferrite in a medium carbon steel, Journal of Materials Science, 40 (2005) 903-908.

[74] Y. Tian, R. Kraft, Kinetics of pearlite spheroidizations, Metallurgical and Materials Transactions A, 18 (1987) 1359-1369.

[75] S.E. Nam, D.N. Lee, Accelerated spheroidization of cementite in high-carbon steel wires by drawing at elevated temperatures, Journal of Materials Science, 22 (1987) 2319-2326.

[76] S.L. Zhang, X.J. Sun, H. Dong, Effect of deformation on the evolution of spheroidization for the ultra high carbon steel, Materials Science and Engineering: A, 432 (2006) 324-332.

[77] A. Kamyabi-Gol, M. Sheikh-Amiri, Spheroidizing Kinetics and Optimization of Heat Treatment Parameters in CK60 Steel Using Taguchi Robust Design, Journal of Iron and Steel Research, International, 17 (2010) 45-52.

[78] Y. Zhang, N. Gey, C. He, X. Zhao, L. Zuo, C. Esling, High temperature tempering behaviors in a structural steel under high magnetic field, Acta Materialia, 52 (2004) 3467-3474.

[79] C.M.B. Bacaltchuk, G.A. Castello-Branco, M. Ebrahimi, H. Garmestani, A.D. Rollett, Effect of magnetic field applied during secondary annealing on texture and grain size of silicon steel, Scripta Materialia, 48 (2003) 1343-1347.

[80] D.S. Li, H. Garmestani, S. Yan, M. Elkawni, M.B. Bacaltchuk, H.J. Schneider-Muntau, J.P. Liu, S. Saha, J.A. Barnard, Effects of high magnetic field annealing on texture and magnetic properties of FePd, Journal of Magnetism and Magnetic Materials, 281 (2004) 272-275.

[81] H.O. Martikainen, V.K. Lindroos., Observations on the effect of magnetic field on the recrystallization in ferrite, Scandinavian Journal of Metallurgy, 10 (1981) 3-8.

[82] K.W. Andrews, The structure of cementite and its relation to ferrite, Acta Metallurgica, 11 (1963) 939-946.

[83] D. Zhou, G. Shiflet, Ferrite: Cementite crystallography in pearlite, Metallurgical and Materials Transactions A, 23 (1992) 1259-1269.

[84] M.X. Zhang, P.M. Kelly, A new orientation relationship between Widmanstatten cementite and austenite, Scripta Materialia, 37 (1997) 2017-2024.

[85] M.X. Zhang, P.M. Kelly, Accurate orientation relationships between ferrite and cementite in pearlite, Scripta Materialia, 37 (1997) 2009-2015.

[86] M.X. Zhang, P.M. Kelly, Crystallography of spheroidite and tempered martensite, Acta Materialia, 46 (1998) 4081-4091.

[87] M.X. Zhang, P.M. Kelly, Crystallography and morphology of Widmanstätten cementite in austenite, Acta Materialia, 46 (1998) 4617-4628.

[88] M. Mangan, G. Shiflet, The pitsch-petch orientation relationship in ferrous pearlite at small undercooling, Metallurgical and Materials Transactions A, 30 (1999) 2767-2781.

[89] M.V. Kral, G. Spanos, Crystallography of grain boundary cementite dendrites, Acta Materialia, 51 (2003) 301-311.

[90] M.X. Zhang, P.M. Kelly, Edge-to-edge matching and its applications, Acta Materialia, 53 (2005) 1085-1096.

[91] M.X. Zhang, P.M. Kelly, Edge-to-edge matching model for predicting orientation relationships and habit planes-the improvements, Scripta Materialia, 52 (2005) 963-968.

[92] A. Walentek, M. Seefeldt, B. Verlinden, E. Aernoudt, P. Vanhoutte, Investigation of pearlite structure by means of electron backscatter diffraction and image analysis of SEM micrographs with an application of the Hough transform, Materials Science and Engineering: A, 483-484 (2008) 716-718.

[93] V. Randle, Electron backscatter diffraction: Strategies for reliable data acquisition and processing, Materials Characterization, 60 (2009) 913-922.

[94] M.X. Zhang, P.M. Kelly, Crystallographic features of phase transformations in solids, Progress in Materials Science, 54 (2009) 1101-1170.

[95] M.X. Zhang, P.M. Kelly, The morphology and formation mechanism of pearlite in steels, Materials Characterization, 60 (2009) 545-554.

[96] R.J. Dippenaar, R.W.K. Honeycombe, The crystallography and nucleation of pearlite Proceedings of the Royal Society of London. Series A, Mathematical and Physical Sciences, 33 (1973) 445-467.

[97] I.V. Isaichev, Orientation between cementite and ferrite, Zhurnal Tekhnicheskoi Fiziki, 17 (1947) 835-838.

[98] Y. Ohmori, Microstructural evolutions with precipitation of carbides in steels, The Iron and Steel Institute of Japan, 41 (2001) 554-565.

[99] Y. Ohmori, A.T. Davenport, R.W.K. Honeycombe, Crystallography of pearlite, Transactions of the Iron and Steel Institute of Japan, 12 (1972) 128-137.

[100] N.J. Petch, The orientation relationships between cementite and α-iron, Acta Crystallographica, 6 (1953) 96.

[101] W. Pitsch, Der Orientierungszusammenhang zwischen Zementit und Ferrit im Perlit, Acta Metallurgica, 10 (1962) 79-80.

[102] Y.A. Bagaryatsky, Veroyatnue mechanezm raspada mar- tenseeta, Doklady Akademii Nauk SSSR, 73 (1950) 1161-1164.

Acknowledgements

This work is financially supported by the National Natural Science Foundation of China (Grant No. 50971034, 50901015 and 50911130365), the Program for Changjiang Scholars and Innovative Research Team in University (Grant No. IRT0713), the “111” Project (Grant No. B07015), the CNRS of France (PICS No. 4164) and the joint Chinese-French project OPTIMAG (N°ANR-09-BLAN-0382). I would like to give my sincere thanks to these institutions. I also gratefully acknowledge the CHINA SCHOLARSHIP COUNCIL for providing the scholarship to support my PhD study in France.

This work is completed at LEM3 (former LETAM, University of Lorraine, France) and the Key Laboratory for Anisotropy and Texture of Materials (Northeastern University, China). I had the honor to work with numerous colleagues in two labs and I would like to give my hearted thanks for their kind help.

I would like to thank the reviewers, Prof. Y. Fautrelle and Prof. Z. M. Ren for taking time out of their busy schedules to review my dissertation and provide constructive suggestions and comments.

I would like to give my special thanks to my supervisors, Prof. Claude Esling, Prof. Yudong Zhang at University of Lorraine, Prof. Liang Zuo and Prof. Xiang Zhao at Northeastern University, not only for their support, ideas, guidance, and organizational help during the last three years, but also making me a better person and scientist by setting high standards and good examples.

I would like to thank all my group members who treated me with dignity and respect.

Last but not least, I want to thank my parents, friends and family, especially my husband Mr. Lijun Zhang for his constant support, understanding and encouragement.

Publications list

Contribution to International Journals

[1] **Xiaoxue Zhang,** Yudong Zhang, Minglong Gong, Claude Esling, Xiang Zhao, Liang Zuo, Effects of a high magnetic field on austenite decomposition in high purity Fe-1.1C (wt.%) alloy, *Materials Science Forum*, 702-703 (2012) 60-63.

[2] **Xiaoxue Zhang,** Yudong Zhang, Shoujing Wang, Claude Esling, Xiang Zhao, Liang Zuo, Effects of magnetic field intensity on microstructure and orientation of proeutectoid ferrite in Fe-C alloy, *Materials Scie*nce *Forum*, 706-709 (2012) 2680-2684

[3] **Xiaoxue Zhang**, Shoujing Wang, Yudong Zhang, Claude Esling, Xiang Zhao, Liang Zuo, Carbon-content dependent effect of magnetic field on austenitic decomposition of steels, *Journal of Magnetism and Magnetic Materials*, 324 (2012) 1385-1390.

[4] Amir Momenil, Kamran Dehghani, **Xiaoxue Zhang**, Mechanical and microstructural analysis of 2205 duplex stainless steel under hot working condition. *Journal of Materials Science,* 47 (2012) 2966-2974,

[5] **Xiaoxue Zhang**, Nan Xu, Shoujing Wang, Yudong Zhang, Jean-Marc Raulot, Claude Esling, Xiang Zhao, Liang Zuo, Magnetic field induced enhancement of carbon content in ferrite, *Applied Physics Letters.* (*Accepted*)

[6] **Xiaoxue Zhang**, Yudong Zhang , Minglong Gong , Claude Esling , Xiang Zhao , Liang Zuo, Effects of a high magnetic field on microstructure in high purity Fe-1.1C (wt.%) alloy during its austenitic decomposition, *Journal of Magnetism and Magnetic Materials. (Accepted)*

Contribution to International Conferences

[1] **Xiaoxue Zhang**, Yudong Zhang, Jianyu Song, Shoujing Wang, Claude Esling, Xiang Zhao, Liang Zuo, *Effect of high magnetic field on high-purity Fe-C alloys during austenitic decomposition*. French-Chinese Symposium on Advanced Materials towards Energy, Transport and Environment, China. 24.05.2010 ~ 26.05.2010.

[2] **Xiaoxue Zhang**, Yudong Zhang, Claude Esling, Xiang Zhao, Liang Zuo, Effects of the high magnetic field on transformed microstructures during austenitic decomposition in high purity Fe-1.1C (wt.%) alloy. *Journées Annuelles de la SF2M 2011*, Nancy, France. 04.07.2011~06.07.2011. ***Oral Presentation***

[3] **Xiaoxue Zhang**, Yudong Zhang, Shoujing Wang, Claude Esling, Xiang Zhao, Liang Zuo, Effects of magnetic field intensity on microstructure and orientation of ferrite in Fe-C alloy. THERMEC' 2011, Québec, Canada. 1.08.2011 ~ 5.08.2011.

[4] **Xiaoxue Zhang**, Yudong Zhang, Minglong Gong, Claude Esling, Xiang Zhao, Liang Zuo, *Effect of a high magnetic field on austenite decomposition in high purity Fe-1.1C (wt.%) alloy*. ICOTOM16, India. 12.12.2011 ~ 17.12.2011.